The mechanics of a trebuchet using Lagrangian mechanics

T.M.A. Levert
(5086191)

BSc Final Project
Faculty of Applied Physics and
Faculty of Applied Mathematics
Delft University of Technology

Delft, 22-06-2022

Supervisors: Dr. B.J. Meulenbroek, Dr. A.F. Otte

Abstract

In this report, we have taken a look at three different types of trebuchets: the seesaw, the traction trebuchet or mangonel, and the counterweight trebuchet. We have created models to describe their motion by making use of Lagrangian mechanics and have compared them based on their maximum ranges. Moreover, we have also calculated a lower bound for the dimensions of the main beam needed to prevent it from breaking based on a static state.

We have seen that the mangonel and trebuchet improved on the seesaw by increasing the range roughly sixfold which was expected. The maximum range of the trebuchet, however, slightly decreased compared to the mangonel. This was something we did not expect but think is due to the fact that the dimensions of the catapults were not optimised.

Lastly, we found that the beam needed to be at least 18.7 cm to prevent it from breaking. However, for the real catapults, the beam would most likely need to be thicker to prevent it from breaking.

Contents

1

Introduction

Validating historical records is often a difficult task. Take for example historical accounts describing a siege of a castle. One might overexaggerate his or her accomplishments or the power of their weapons. Moreover, they might use different units of measurement which further complicates the validation of the source. Imagine an account where they describe the abilities of their siege weapon: how far it can shoot, the impact it had on the castle, the dimensions of the weapon, etc. The credibility of this source can be hard to determine without any other sources or rebuilding the weapon. Sometimes, other sources are not available and rebuilding such large machines is often very cumbersome. A solution could be to create mathematical models to try and determine if the claims made can be truthful. This paper aims to develop such models for different types of old siege weapons in order to analyse their movements. This could be used in order to, for example, validate historical sources and therefore obtain a better understanding of old civilizations and the attention they gave to warfare.

In this chapter we start by looking at the history of the trebuchet and how it works in section 1.1, then we will talk about the aim of the paper and the assumptions we make to obtain this. We will end with the nomenclature that will be used throughout the paper and the structure of the remaining paper.

1.1. The trebuchet and its origins

1.1.1. The evolution

A trebuchet is a collective name for different kinds of catapults used for siege warfare. They were most prominent during the Middle Ages but were already used in China around the fourth century BC [1]. Their main use was as artillery to attack settlements or castles from a safe distance. They could damage walls or destroy buildings within the surrounding walls and therefore make it possible to more easily invade these settlements or castles.

The main predecessors of the trebuchet were the ballista and the torsion-powered catapult [1]. The trebuchet differs from them by how they store the potential energy which is used to launch the projectile. The ballista and torsion-powered catapult depend on tension in a rope which is used for launch; much like a bow and arrow. The trebuchet, on the other hand, saves the potential energy by lifting a large counterweight into the air and dropping it, subsequently launching the projectile into the air. This allowed more potential energy to be stored in the system as it did not rely on the strength of the rope and was more easily scalable. As a consequence, the trebuchet could fire heavier projectiles and could more easily destroy castle walls than either the ballista or the torsion-powered catapult.

As mentioned, the word "trebuchet" is actually a collective name for several types of catapults. The common factors between these different types are that they do not rely on tension in ropes but rather on the potential energy due to a counterweight being lifted off the ground and that they all have an arm that pivots. So in general, all trebuchets have a long beam that was placed off-centre on a pivot which was on a large base to support the entire machine. The short end of the beam was where the counterweight was attached and the long end, or throwing arm, held the projectile. The counterweight would often be very heavy to maximize the potential energy in the system. Also, a longer throwing arm would be used as this increased the range.

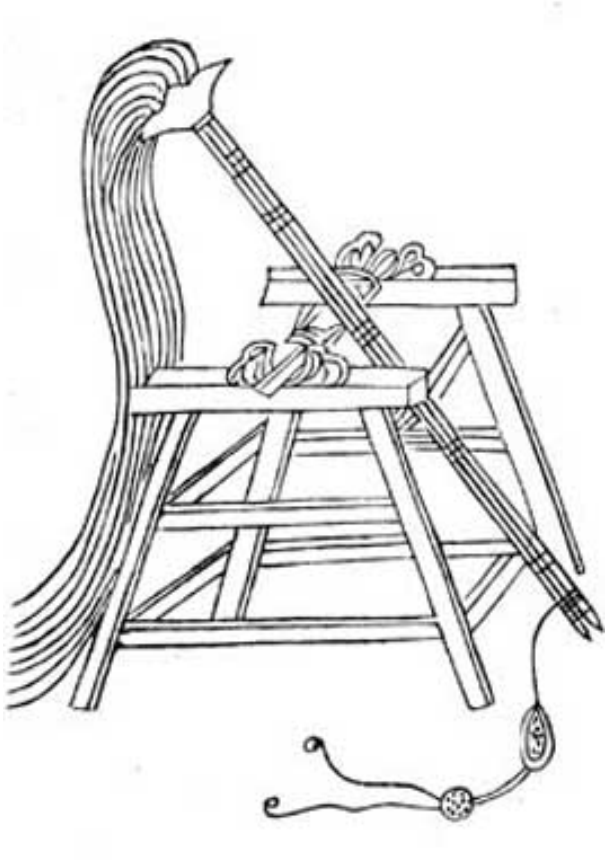

Figure 1.1: A drawing of an original mangonel where the beam would be pulled down by soldiers rather than by a counterweight. The projectile would be put in the sling which is depicted in the bottom right. The updated mangonel which had a fixed counterweight would have had the counterweight where the pulling ropes are now attached. [2]

By adding elements to this basic structure different trebuchets can be created. The first trebuchet was the traction trebuchet, also called the mangonel. It consisted of the beam as mentioned earlier and a rope which connected the projectile to this beam. The original mangonel relied on manpower rather than a counterweight. A picture of such a mangonel can be seen in figure 1.1. Up to 250 soldiers would pull down on the short end of the beam in order to launch the projectile [3]. This was very inefficient and difficult to aim since the pulling force of the men was not consistent. Therefore, the soldiers were soon replaced by a fixed counterweight. This made the machine easier to operate and far more accurate.

After the mangonel, the counterweight trebuchet, or more generally just the trebuchet, came around. This trebuchet relied on a hinged counterweight but other than that was the same as the mangonel. This hinged counterweight reduced the movement of the system at the moment the projectile was fired. This meant more of its stored energy was transferred into the projectile making it more efficient. Moreover, the hinged counterweight also increased the accuracy of the trebuchet as it reduced the strain in the system. The Museum of Falsters Minder in Denmark has made a medium-sized reconstruction which could fire its projectiles within a six-meter square over a range of 180m consistently [4]. A picture of a trebuchet can be seen in figure 1.2.

Figure 1.2: A drawing of a counterweight trebuchet. Note the hinged counterweight which is the main change compared to the updated mangonel which had a fixed counterweight. [5]

1.1.2. Mechanics of the trebuchet

As we discussed above there are different types of trebuchets. We will look at three different types: the seesaw, the mangonel with a fixed counterweight, and the counterweight trebuchet. The seesaw is just the main beam as described above, and thus the most simple type of trebuchet. The projectile of the seesaw is therefore not connected by a rope to the beam but rather is attached straight to the beam. Also, its counterweight is fixed and not hinged.

The firing process of all catapults can be split into three distinct phases: the projectile is sliding through a trough on the ground (phase I), the projectile has come off the ground but is still attached to the catapult (phase II), the projectile is released from the catapult (phase III). Since the seesaw has no rope phase I is not present as the projectile gets off the ground as soon as the seesaw starts rotating. The movement of the catapults is different for all the distinct phases and thus it is important to look at these phases separately. During phase I the projectile is dragged along the trough on the ground. In phase II the projectile has come off the ground but has not yet been shot. In figure 1.3 we can see the transition from the initial condition to phase I and then to phase II.

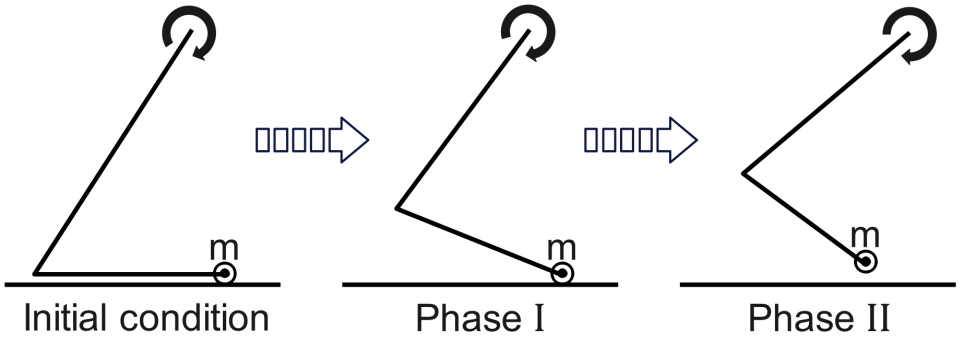

Figure 1.3: In this figure the transition from phase I to phase II is shown. Part of the main beam as well as the rope and the projectile is shown. On the left, we have the initial condition. In the middle, we see that the catapult has started rotating and that the projectile is being dragged along the trough. This depicts the catapult in phase I. Lastly, on the right, we have a snapshot of the catapult when it has just moved into phase II and thus the projectile has lifted off the ground.

Lastly, we have phase III where the projectile has been shot and is no longer attached to the catapult.

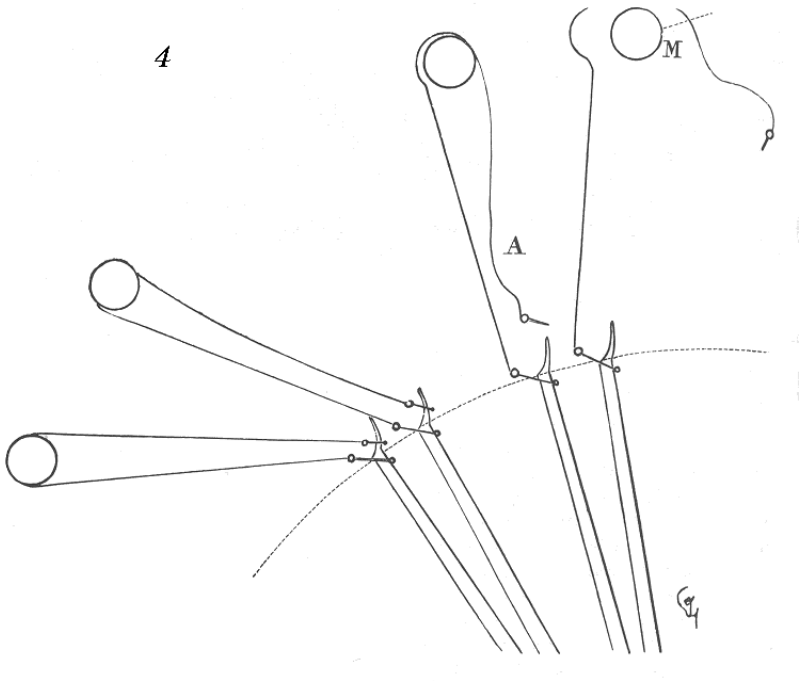

Figure 1.4: The release mechanism used for the mangonel and trebuchet. Note that the projectile is in a pouch of a sling and one end of the sling is permanently attached to the beam. The other end of the sling is hooked on a pin of which the angle with the main beam can be adjusted. [6]

Although, the movement of the catapult is no longer of the greatest interest it could still be important for, for example, calculating if the beam were to break. More relevant, however, is how we know when the projectile is being launched. For the seesaw, it can be done in different ways. The most common of which is to limit the angle the beam can make by, for example, letting it hit a crossbeam. This causes the beam to abruptly stop which, as a consequence, shoots the projectile.

For the mangonel and the trebuchet, it is a bit more complex to know how and when the projectile is released. It is important to understand how the projectile is attached to the main beam of the catapult. The release mechanism is shown in figure 1.4. One end of the sling is permanently attached to the main beam while the other end is hooked onto a pin. The angle the pin makes with the beam can be adjusted. By changing this angle the operator of the catapult can determine at which angle the sling comes off the pin and the projectile is released. This allows the mangonel and trebuchet to accurately aim and change their range.

1.2. Research question and assumptions

We now know how the catapults work and the different phases we need to look at. In this paper, we will seek to develop a model to simulate the movements of the seesaw, mangonel, and trebuchet while firing. We will do this by making use of the theory of Lagrangian mechanics which will be explained in section 2.1.

In order to realise this model, we make several assumptions. This is needed to make the model manageable and usable. The assumptions we will make are the following: the projectile nor the catapult experience air resistance, the joints of the catapult are frictionless (therefore no damping occurs), and the sling with which the projectile is attached to the mangonel or trebuchet is massless and is considered rigid.

The fact that there is no air resistance and no friction allows us to use a more simple variant of Lagrangian mechanics. If we were to include friction we would have to resort to either a time-dependent Lagrangian or a dissipation function. The massless and rigid rope reduces the number of coordinates and therefore simplifies the calculations. We will come back to the effect of these assumptions in the discussion in chapter 8.

Variable	Definition	Unit	Used value
Lengths			
L_1	Distance from the pivot point of the main beam to the attachment of the counterweight	m	1.2
L_2	Distance from the pivot point of the main beam to the attachment of the projectile	m	5.7
L_3	Length of the sling	m	5.0
L_b	Distance from the pivot point of the main beam to its cenre of mass	m	2.25
L_M	Length of the beam connecting the counterweight to the main beam	m	1.4
H	Height of the pivot point of the main beam compared to the ground	m	3.2 $H \geq L_1 + L_M$
b	Width and height of the main beam	m	–
Masses			
m	Mass of the projectile	kg	15
M	Mass of the counterweight	kg	2000
m_b	Mass of the main beam	kg	300
Angles			
θ_0	Initial angle of the main beam with the vertical	rad	$\cos^{-1}\left(\frac{H}{L_2}\right) = 0.975$
$\dot{\theta}_0$	Initial angular velocity of the main beam	rad/s	0
α_0	Initial angle of the sling with the main beam	rad	$\frac{\pi}{2} - \theta_0 = 0.596$
$\dot{\alpha}_0$	Initial angular velocity of the sling	rad/s	0
ϕ_0	Initial angle of the counterweight beam with the main beam	rad	$\theta_0 = 0.975$
$\dot{\phi}_0$	Initial angular velocity of the counterweight	rad/s	0
θ_r	Release angle for the seesaw	rad	–, $\theta_0 \leq \theta_r \leq 2\pi - \theta_0$
α_r	Release angle for the mangonel and trebuchet	rad	–
Miscellaneous			
g	Gravitational acceleration	m/s^2	9.81
I	Second moment of area of the beam	m^4	$\frac{1}{12}b^4$
I_b	Moment of inertia of the beam	kg· m^2	$m_b(\frac{1}{12}(L_1 + L_2)^2 + L_b^2) = 0.269$
σ	Yield stress	Pa	$70 \cdot 10^6$

Table 1.1: The nomenclature used throughout this paper with the values that are being used denoted. We refer to figures 3.1, 4.1, and 5.1 for a visual representation of the definitions of the angles and lengths. If the value is denoted by – this means we use this as a variable and if used as a fixed value we will mention this. Moreover, if we deviate from the values given above we will also explicitly mention this. There are several assumptions we make within this table. Namely, that the beam has an equal weight distribution which gives rise to the definition used for I_b and that the beam is square with both sides having dimension b which in turn gives rise to the definition for I. Additionally, we assume the counterweight to be maximally raised, thus the end of the beam touches the ground which results in the definition of θ_0 being used. Due to the conservation of energy the release angle, θ_r, for the seesaw needs to be in the interval $[\theta_0, 2\pi - \theta_0]$. We also assume that the counterweight is hanging straight down from the main beam which results in $\phi_0 = \theta_0$. Moreover, we assume that the sling is parallel to the ground, again giving rise to the definition used for α_0. Lastly, we need that $H \geq L_1 + L_M$ since otherwise, the counterweight would hit the ground. We do not take into account the shape of the counterweight but instead require the cenre of mass of the counterweight not to hit the ground.

1.3. Nomenclature

Throughout this paper, we will be using the notation as described in table 1.1. After this chapter, we will first discuss the theory on which the models are based in chapter 2. Chapters 3, 4, and 5 will show the formulation of the models for the seesaw, mangonel, and trebuchet respectively. Not all calculations will be shown in full in these chapters but can instead be found in the appendix. The results for the different siege weapons will be discussed in chapter 6. We will also calculate a lower bound for how big the main beam needs to be to prevent it from breaking. The theory for this will also be discussed in chapter 2 and its results are shown in chapter 7. Lastly, the discussion and conclusion will be presented in chapters 8 and 9 respectively.

2

Theoretical concepts used

In this chapter we will discuss the theory used to solve the problem at hand. We will make some remarks and explain the underlying principles used in the rest of this paper. We will explain the main theories used in this paper in this chapter. The theory of Lagrangian mechanics is explained in section 2.1 and the theory of bending moments in section 2.2.

2.1. Lagrangian mechanics

Most people are familiar with Newtonian mechanics where forces are used to derive the equations of motion from which we can determine how an object will move. The downside of this method is that we always need to know the forces acting on an object which makes it very cumbersome for complex systems like siege weapons. Unlike Newtonian mechanics, Lagrangian mechanics only needs the energy of the system as function of its coordinates and can make use of generalised coordinates. This is an advantage in our case since this makes the problem at hand easier to solve as it reduces the number of coordinates we need to keep track of and eliminates the need to know the forces acting on the system. Moreover, the method of Lagrangian multipliers allows us to introduce constraint forces without explicitly knowing the exact force at any given time, which will be explained in section 2.1.2. We will use this theory in chapters 3, 4, and 5.

Lagrangian mechanics makes use of the stationary action principle which suggests that the action functional of a system must stay at a stationary point as time moves on. This is a physical concept and not a mathematical theorem or requirement. In essence, it says that in nature objects move according to the path of least resistance. Although somewhat empirical of nature we see this principle comes back in many areas of physics. Take for example refraction in optics. Here light follows the path from A to B that takes the least amount time. Even the fact that a straight line is the shortest path from A to B is based on this principle. The action on which this theory is based is defined as

$$S = \int_{t_1}^{t_2} \mathscr{L}\, dt = \int_{t_1}^{t_2} T - U dt \tag{2.1}$$

and $\mathscr{L}$ is called the Lagrangian and is the action functional. T is the kinetic energy and U is the potential energy in Joules. By applying the principle of least action on equation 2.1 we can obtain the Euler-Lagrange equation which in turn gives us the equations of motion.

2.1.1. Euler-Lagrange equation

We will now explain the Euler-Lagrange equation and show the mathematical proof. The steps displayed here are mostly taken from [7].

Suppose we have a function $x(t)$ which describes the path of the object we are taking a look at and assume that this is the right path and thus satisfies the principle of least action. Suppose now that we have an arbitrary function $\zeta(t)$ which is a deviation to this correct path. Where $\zeta(t_1) = \zeta(t_2) = 0$ to ensure we start and end at the same point. We can then define the new path as $X(t) = x(t) + \beta\zeta(t)$ with β being some real number. Note that $\beta = 0$ gives us the correct path again. Generally, the Lagrangian is defined by the path and the derivative of the path. This makes sense since the kinetic energy is dependent on the speed, or the derivative of the path, and

the potential energy is often dependent only on the path itself. Therefore $\mathscr{L} = \mathscr{L}(X, \dot{X}, t)$ and thus the action can be written as

$$S(\beta) = \int_{t_1}^{t_2} \mathscr{L}(X, \dot{X}, t)\, dt \tag{2.2}$$

Since we want to find a stationary point for S and know we get this for $\beta = 0$ since then $X = x$ where x is the correct path we need that

$$\frac{dS}{d\beta} = \int_{t_1}^{t_2} \frac{\partial}{\partial \beta} \mathscr{L}\left(x(t) + \beta\zeta(t), \dot{x}(t) + \beta\dot{\zeta}(t), t\right) dt = 0 \tag{2.3}$$

Note this gives us a stationary point for S but not necessarily a minimum or maxima. However, it is not required to have a minima or maxima bur rather that S is stationary. By using the chain rule we can obtain that

$$\frac{\partial \mathscr{L}\left(x(t) + \beta\zeta(t), \dot{x}(t) + \beta\dot{\zeta}(t), t\right)}{\partial \beta} = \zeta(t)\frac{\partial \mathscr{L}}{\partial x} + \dot{\zeta}(t)\frac{\partial \mathscr{L}}{\partial \dot{x}} \tag{2.4}$$

We can rewrite the integral over the second term of equation 2.4 by using integration by parts.

$$\int_{t_1}^{t_2} \dot{\zeta}(t)\frac{\partial \mathscr{L}}{\partial \dot{x}} dt = \left[\zeta(t)\frac{\partial \mathscr{L}}{\partial \dot{x}}\right]_{t_1}^{t_2} - \int_{t_1}^{t_2} \zeta(t)\frac{d}{dt}\frac{\partial \mathscr{L}}{\partial \dot{x}} dt \tag{2.5}$$

Given the conditions on ζ, $\zeta(t_1) = \zeta(t_2) = 0$, the first term on the right hand side of equation 2.5 evaluates to zero. Combining this with what we have found so far we get

$$\frac{dS}{d\beta} = \int_{t_1}^{t_2} \zeta(t)\left(\frac{\partial \mathscr{L}}{\partial x} - \frac{d}{dt}\frac{\partial \mathscr{L}}{\partial \dot{x}}\right) dt = 0 \tag{2.6}$$

Since this needs to hold for all $\zeta(t)$ we can conclude

$$\frac{\partial \mathscr{L}}{\partial x} - \frac{d}{dt}\frac{\partial \mathscr{L}}{\partial \dot{x}} = 0 \tag{2.7}$$

which is called the Euler-Lagrange equation.

Suppose now that we have that the Lagrangian depends on more than one variable that all depend on the time t: $x_1(t), x_2(t), \ldots$. We can repeat the above steps for all these different variables. This gives us

$$\frac{\partial \mathscr{L}}{\partial x_i} - \frac{d}{dt}\frac{\partial \mathscr{L}}{\partial \dot{x}_i} = 0 \tag{2.8}$$

We can now see that given the Lagrangian we are able to find ordinary differential equations for the problem at hand. However, for the mangonel and the trebuchet we will need an addition to this theory. Namely, we will have to deal with some constraints.

2.1.2. Lagrange multiplier

In particular, let us assume we have a holonomic constraint. A holonomic constraint is a constraint that can be written in the following form

$$f(x_1, x_2, \ldots) = \text{const.} \tag{2.9}$$

Note that a holonomic constraint does only depend on the coordinates themselves and not the time derivatives of these coordinates, without this fact we could not take the step which results in equation 2.14. It is important to note that we cannot just take any constraint force into account. Lagrangian multipliers are only able to incorporate conservative forces, so not friction or air resistance. This is due to the fact that non-conservative forces are dependent on the path followed. Let us now define a new Lagrangian where we only look at two coordinates without loss of generality for simplicity

$$\mathscr{L}'\big(x(t), y(t), \dot{x}(t), \dot{y}(t), t\big) = \mathscr{L}\big(x(t), y(t), \dot{x}(t), \dot{y}(t), t\big) - \lambda(t) f\big(x(t), y(t), t\big) \tag{2.10}$$

where $\mathscr{L}$ is the Lagrangian as defined previously in equation 2.1 and λ some parameter dependent on time called the Lagrange multiplier. If we again have a deviation $\zeta_x(t)$ to the correct path $x(t)$ and a deviation $\zeta_y(t)$ to $y(t)$ where we have $\zeta_i(t_1) = \zeta_i(t_2) = 0$,we get that

$$\mathscr{L}'\left(X, Y, \dot{X}, \dot{Y}, t\right) = \mathscr{L}\left(x + \beta\zeta_x, y + \beta\zeta_y, \dot{x} + \beta\dot{\zeta_x}, \dot{y} + \beta\dot{\zeta_y}, t\right) - \lambda(t) f\left(x + \beta\zeta_x, y + \beta\zeta_y, t\right) \tag{2.11}$$

Again we have that the derivative with respect to β of the action over $\mathscr{L}'$ has to be equal to zero by the stationary action principle as we showed in equation 2.3. Using the chain rule we now see

$$\frac{\partial \mathscr{L}'}{\partial \beta} = \zeta_x(t)\frac{\partial \mathscr{L}'}{\partial x} + \dot{\zeta}_x(t)\frac{\partial \mathscr{L}'}{\partial \dot{x}} + \zeta_y(t)\frac{\partial \mathscr{L}'}{\partial y} + \dot{\zeta}_y(t)\frac{\partial \mathscr{L}'}{\partial \dot{y}} \tag{2.12}$$

Equivalent to the step taken in equation 2.5 we rewrite the integral over equation 2.12 by using integration by parts which eventually results in

$$\frac{dS}{d\beta} = \int_{t_1}^{t_2} \zeta_x(t)\left(\frac{\partial \mathscr{L}'}{\partial x} - \frac{d}{dt}\frac{\partial \mathscr{L}'}{\partial \dot{x}}\right)dt + \int_{t_1}^{t_2} \zeta_y(t)\left(\frac{\partial \mathscr{L}'}{\partial y} - \frac{d}{dt}\frac{\partial \mathscr{L}'}{\partial \dot{y}}\right)dt = 0 \tag{2.13}$$

Using that $\mathscr{L}' = \mathscr{L} - \lambda f$ and that f is independent of $\dot{x}$ and $\dot{y}$ we can write equation 2.13 out giving us

$$\frac{dS}{d\beta} = \int_{t_1}^{t_2} \zeta_x(t)\left(\frac{\partial \mathscr{L}}{\partial x} - \lambda(t)\frac{\partial f}{\partial x} - \frac{d}{dt}\frac{\partial \mathscr{L}}{\partial \dot{x}}\right)dt + \int_{t_1}^{t_2} \zeta_y(t)\left(\frac{\partial \mathscr{L}}{\partial y} - \lambda(t)\frac{\partial f}{\partial y} - \frac{d}{dt}\frac{\partial \mathscr{L}}{\partial \dot{y}}\right)dt = 0 \tag{2.14}$$

Now the importance of the Lagrange multiplier comes into play. Let us choose $\lambda(t)$ such that the coefficient of $\zeta_x(t)$ in the first integral of equation 2.14 becomes zero. Then the whole first integral evaluates to zero and thus so must the second integral. Therefore, we end up with

$$\frac{\partial \mathscr{L}}{\partial x} - \lambda(t)\frac{\partial f}{\partial x} - \frac{d}{dt}\frac{\partial \mathscr{L}}{\partial \dot{x}} = 0 \tag{2.15}$$

and

$$\frac{\partial \mathscr{L}}{\partial y} - \lambda(t)\frac{\partial f}{\partial y} - \frac{d}{dt}\frac{\partial \mathscr{L}}{\partial \dot{y}} = 0 \tag{2.16}$$

We now have three unknown functions: $x(t)$, $y(t)$ and $\lambda(t)$. In general, this is solvable if we have three equations. Fortunately, we have three equations, namely, equations 2.9, 2.15, and 2.16. Since we use equation 2.9 in order to obtain our solution it ensures that the constraint will be met.

We can now also find out what the constraint forces are. If we remember that $\mathscr{L} = T - U$ as we defined in equation 2.1 and that, in general, $T = T(\dot{x}, \dot{y}, t)$ and $U = U(x, y, t)$ we can substitute this into equation 2.15 which results in

$$-\frac{\partial U}{\partial x} - \lambda\frac{\partial f}{\partial x} - \frac{d}{dt}\frac{\partial T}{\partial \dot{x}} = 0 \tag{2.17}$$

Note that in the most general case $T = \frac{1}{2}m_1\dot{x}^2 + \frac{1}{2}m_2\dot{y}^2$ since the coordinates do not necessarily have to be linked to the same object. This simplifies the last term of equation 2.17 to

$$\frac{d}{dt}\frac{\partial T}{\partial \dot{x}} = m_1\ddot{x} \tag{2.18}$$

Note that this is x-component of the total force on m_1 which is the sum of the non-constraint and constraint forces, or

$$m_1\ddot{x} = -\frac{\partial U}{\partial x} + F_x^{\text{constraint}} \tag{2.19}$$

Where $F_x^{\text{constraint}}$ is the constraint force in the x direction. Combining equations 2.17, 2.18, and 2.19 we obtain that

$$-\lambda\frac{\partial f}{\partial x} = F_x^{\text{constraint}} \tag{2.20}$$

Or in the general case that

$$-\lambda\frac{\partial f}{\partial x_i} = F_{x_i}^{\text{constraint}} \tag{2.21}$$

We can now include holonomic constraints and see what the forces due to this constraint are. This will be helpful later in chapters 4 and 5 where we will analyse the mangonel and trebuchet.

2.2. Bending moment

We have now discussed the theory to determine the movement of the catapults. However, from a more practical perspective we are interested in how we should manufacture such a catapult. Certainly, it is important that the trebuchet will not break when using it. To see when it will break we would need to do some extensive calculations which go beyond the scope of this paper. Therefore, we will calculate a lower bound for the dimensions of the main beam needed to prevent it from breaking. The difficulty in calculating the exact dimensions needed lies in the fact that it is a dynamic system. For the lower bound, we will therefore look at the static case. For the dynamic case the forces will be greater as the rotation will cause extra stresses in the material and therefore we can take the static case as a lower bound.

In order to see if a static beam will break under stress we need to look at the bending moment in that beam. The bending moment is related to the tensile and compressive forces present in a beam. Therefore, if the bending moment induces tensile or compressive forces larger than the beam's yield stress the beam will break.

Remember that a moment is the cross product between a force and the distance from the reference point. The bending moment is similar to the moment but is a function describing the moment experienced at any point in the beam. Therefore, by taking the left side of the beam as the origin the bending moment is defined as

$$M(x) = \int_0^x V(x)\,dx \tag{2.22}$$

Here $V(x)$ is the shear force at point x and is given by adding all forces left of x. The maximum bending moment of a beam can be found by making use of shear moment diagrams in which the forces are drawn and then the bending moment at any given point is calculated by making use of equation 2.22. An example of such a shear moment diagram is shown in figure 2.1.

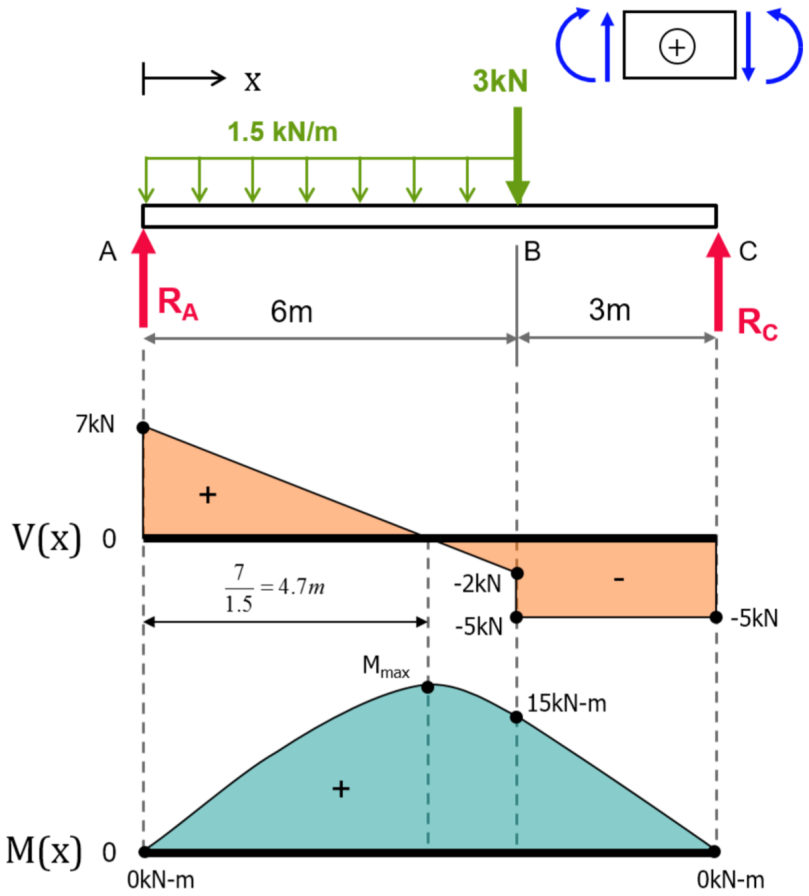

Figure 2.1: An example of a shear moment diagram made by [8]. At the top we can see the forces acting on the beam which is supported on both sides at locations A and C. In the middle we see the shear diagram which shows how the forces propagate through the beam. At the bottom the moment diagram is displayed which shows the bending moment at any given point in the beam. This figure has been modified by cropping some of the image.

We will apply the same principle to our problem. We will only look at the bending moment of the main beam as this will have the most forces on it and is therefore most likely to break. If we look at the forces perpendicular to the beam we can create a similar image to that of figure 2.1. We do this by assuming the beam to be horizontal as this maximizes the gravitational force perpendicular to the beam. This gives us a moment diagram from which we can read the maximum bending moment M_{max}.

For brittle materials, such as wood, we know that if the bending moment gets higher than the moment it can handle, M_{break}, the beam breaks. M_{break} is given by

$$M_{break} = \frac{\sigma I}{y} \tag{2.23}$$

where σ is the yield stress of the beam, I is the second moment of area around the neutral axis and y is the maximum perpendicular distance from the neutral axis to an extremity of the beam's cross section. The neutral axis is the axis of the beam that does not change in length due to bending. For a rectangular beam with width b and height h we have $I = \frac{1}{12}bh^3$ and $y = \frac{h}{2}$. The yield stress is dependent on the material of the beam and is thus also dependent on the species of wood used. For the purposes of this paper we will be assuming the trebuchets to be made of beech wood or more precisely wood from the species *Fagus sylvatica*. We choose this wood type since it is broadly available wood in Europe and is relatively strong. This species of wood has a yield strength of $\sigma = 40$ N/mm^2 [9]. If now $M_{max} \geq M_{break}$ we conclude the beam breaks.

3

Seesaw

In this chapter, we will apply the theory from section 2.1 to the seesaw catapult. The results of this chapter can be found in section 6.1. Before diving into the Lagrangian mechanics we will start by taking a look at the seesaw itself and look at how it works intuitively. After making some key remarks on the seesaw we will find the coordinates of the different masses which we will need to calculate the Lagrangian. Once we have found the Lagrangian we can use the Euler-Lagrange equation (equation 2.8) to get our ODE for the movement of the seesaw.

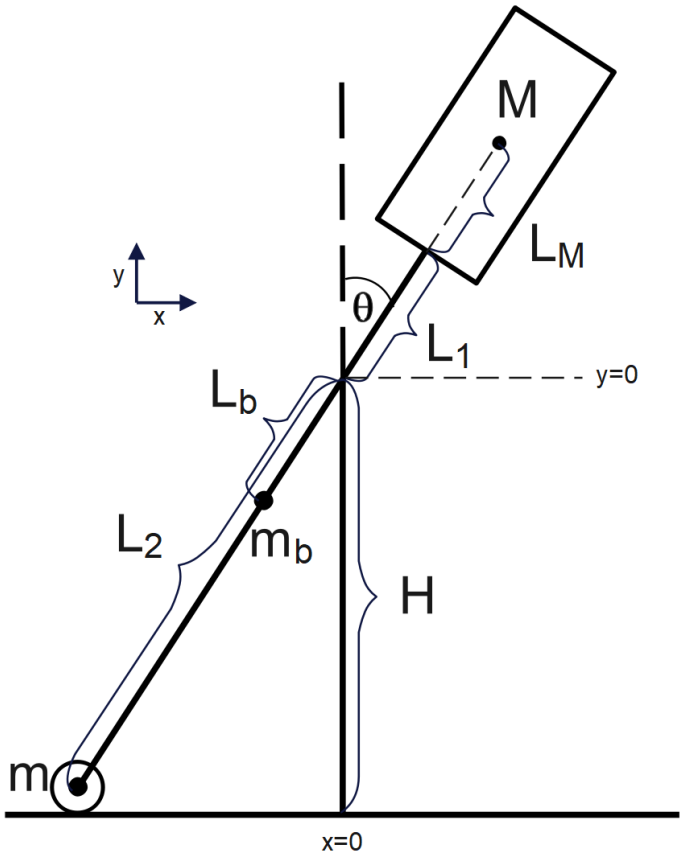

Figure 3.1: Schematic representation of the seesaw with all the variables defined as in table 1.1. The main beam rotates around the origin and the lengths are all fixed. As we can see all the coordinates can be expressed using θ. θ is the only variable dependent on time while all the other variables are fixed constants.

When looking at figure 3.1 we see a schematic representation of the seesaw. Essentially, it is a beam rotating around a pivot point with two masses on either side. The beam will rotate if the moments on the beam are not

in equilibrium. This rotation and therefore the whole system can be described by the angle θ as a function of time since the length of the beam itself is fixed. Therefore, θ is the only generalised coordinate we will use for the seesaw. Let us now define the coordinates of the masses and their velocities. We again refer to figure 3.1 to see how the angles, masses and lengths are defined. All the coordinates are obtained by making use of basic trigonometry. For the counterweight we have

$$\begin{cases} x_M = \sin(\theta)(L_1 + L_M) & \implies \quad \dot{x}_M = \dot{\theta}\cos(\theta)(L_1 + L_M) \\ y_M = \cos(\theta)(L_1 + L_M) & \implies \quad \dot{y}_M = -\dot{\theta}\sin(\theta)(L_1 + L_M) \end{cases} \tag{3.1}$$

where $\dot{x}_M$ and $\dot{y}_M$ are the time derivatives of the coordinates. Similarly, for the projectile we have

$$\begin{cases} x_m = -\sin(\theta)L_2 & \implies \quad \dot{x}_m = -\dot{\theta}\cos(\theta)L_2 \\ y_m = -\cos(\theta)L_2 & \implies \quad \dot{y}_m = \dot{\theta}\sin(\theta)L_2 \end{cases} \tag{3.2}$$

Lastly for the center of mass (COM) of the beam we have

$$\begin{cases} x_b = -\sin(\theta)L_b \\ y_b = -\cos(\theta)L_b \end{cases} \tag{3.3}$$

Note that we do not define the time derivative of the coordinates for the COM of the beam since the kinetic energy of the beam is given by $\frac{1}{2}I_b\dot{\theta}^2$ where I_b is the moment of inertia of the beam. This is because we do not assume the beam to be a point mass but rather a body with a mass.

Let us also define the initial conditions. At $t = 0$ the seesaw starts in rest and therefore $\dot{\theta}_0 = 0$. Moreover, at $t = 0$ we have $\theta_0 \geq \cos^{-1}\left(\frac{H}{L_2}\right)$ since the projectile cannot be underground. We will always take θ to be equivalent to the inverse cosine as this maximises its initial energy. However, if $H > L_2$ the inverse cosine does not exist and thus θ_0 is free. In our case, we always assume $H \leq L_2$ to prevent this problem. We also know the release condition, namely $\theta = \theta_r$. As soon as this is the case we move into phase III.

Now that we have defined the coordinates and initial conditions we can continue with the Lagrangian and the Lagrangian mechanics. As we discussed in section 1.1.2 the firing process of the seesaw has two phases: phase II and phase III. We will approach each phase separately. Phase II will be discussed in section 3.1 and phase III will be discussed in section 3.2.

3.1. Phase II

We want to find the solutions to the ODE obtained by using the Euler-Lagrange equation. In order to do this, we will need to first find the Lagrangian and thus the kinetic and potential energy. In phase II the kinetic energy is given by

$$T = \frac{1}{2}\left(M(\dot{x}_M^2 + \dot{y}_M^2) + m(\dot{x}_m^2 + \dot{y}_m^2) + I_b\dot{\theta}^2\right) \tag{3.4}$$

When substituting equations 3.1, 3.2, and 3.3 into equation 3.4 this reduces to

$$T = \frac{1}{2}\dot{\theta}^2\left(M(L_1 + L_M)^2 + I_b + mL_2^2\right) \tag{3.5}$$

The potential energy is given by

$$U = g\left(My_M + m_b y_b + my_m\right) \tag{3.6}$$

which, after substituting equations 3.1, 3.2, and 3.3 into equation 3.6, simplifies to

$$U = g\cos(\theta)\left(M(L_1 + L_M) - m_b L_b - mL_2\right) \tag{3.7}$$

This gives us our Lagrangian

$$\mathscr{L} = T - U = \frac{1}{2}\dot{\theta}^2\left(M(L_1 + L_M)^2 + I_b + mL_2^2\right) - g\cos(\theta)\left(M(L_1 + L_M) - m_b L_b - mL_2\right) \tag{3.8}$$

Now that we have found our Lagrangian we can use it in the Euler-Lagrange equation. Using θ as the coordinate the Euler-Lagrange equation (equation 2.8) turns into

$$\frac{d}{dt}\frac{\delta\mathscr{L}}{\delta\dot{\theta}} - \frac{\delta\mathscr{L}}{\delta\theta} = 0 \tag{3.9}$$

When substituting equation 3.8 into equation 3.9 we get an ODE for θ, namely equation 3.10. This is obtained simply by taking the derivatives and solving for $\ddot{\theta}$. Once we have it in this form we can numerically solve it to get $\theta(t)$.

$$\ddot{\theta} = g\frac{M(L_1 + L_M) - m_b L_b - mL_2}{M(L_1 + L_M)^2 + I_b + mL_2^2}\sin(\theta) \equiv K\sin(\theta) \tag{3.10}$$

For the seesaw, however, we are able to get an exact solution for $\dot{\theta}$ as a function of θ. By doing this we only need to solve one ODE numerically rather than two to obtain our direct solution for θ. By integrating equation 3.10 multiplied by $\dot{\theta}$ we can get an equation for the angular velocity $\dot{\theta}$.

$$\int \ddot{\theta}\dot{\theta}\,dt = \int K\sin(\theta)\dot{\theta}\,dt \tag{3.11}$$

$$\frac{1}{2}\dot{\theta}^2 = -K\cos(\theta) + \tau \tag{3.12}$$

Using the initial condition $\dot{\theta}_0 = 0$ and inserting this into equation 3.12 we get $\tau = K\cos(\theta_0)$. This results in

$$\dot{\theta} = \pm\sqrt{-2K(\cos(\theta) - \cos(\theta_0))} \tag{3.13}$$

Here we have to use the positive function since we expect $\dot{\theta} > 0$ prior to firing the projectile. This gives us the intermediate solution for $\dot{\theta}$ as a function of θ, namely equation 3.14.

$$\dot{\theta} = \sqrt{-2K(\cos(\theta) - \cos(\theta_0))} \tag{3.14}$$

Note that this could give rise to problems if $-2K(\cos(\theta) - \cos(\theta_0)) < 0$. Luckily, this does not happen as it would require the counterweight to get higher than its initial position which would violate the conservation of energy. Mathematically we can prove this as well. Firstly, $K > 0$ as we assume that the counterweight will drop down and therefore $M(L_1 + L_M) > m_b L_b + mL_2$. Secondly, $\cos(\theta) - \cos(\theta_0) > 0$ only if $2\pi - \theta_0 < \theta \leq 2\pi$ or $0 \leq \theta < \theta_0$. Since the motion of the seesaw is not driven by an external force we know θ can never get in either of these two ranges due to the conservation of energy.

It would be possible to find a direct formula for θ as a function of t. However, this would leave us with an unpleasant integral which would still need to be evaluated numerically. So for the sake of simplicity, we will stop at this stage.

Now we have found the Lagrangian for the seesaw in phase II and used it in the Euler-Lagrange equation to find our ODE for θ. We saw that we could also find the exact solution for $\dot{\theta}$ as a function of θ. This allows us to obtain $\theta(t)$ numerically.

3.2. Phase III

In the previous section, we have found the equations of motion for the seesaw during phase II. We have also defined the release condition for the projectile, namely $\theta = \theta_r$. So as soon as this condition is met we move into phase III where the projectile is released and therefore the Lagrangian changes. We will first look at the trajectory followed by the projectile, after which we will again find the equations of motion for the seesaw during this phase.

At release angle θ_r the projectile is no longer attached to the seesaw and therefore its trajectory is set as it has no forces other than gravity acting upon it. By making use of equations 3.2 and 3.14 we know that at at $\theta = \theta_r$

$$\dot{x}_m = -\cos(\theta_r)L_2\sqrt{-2K(\cos(\theta_r) - \cos(\theta_0))} \tag{3.15}$$

$$\dot{y}_m = \sin(\theta_r)L_2\sqrt{-2K(\cos(\theta_r) - \cos(\theta_0))} \tag{3.16}$$

$$\tag{3.17}$$

Since we assume the projectile to be in a free fall with an initial location and velocity we know $\ddot{x}_m = 0$ and $\ddot{y}_m = -g$. Therefore the trajectory is given by

$$x_m(t) = -\sin(\theta_r)L_2 - t\cos(\theta_r)L_2\sqrt{-2K(\cos(\theta_r) - \cos(\theta_0))} \tag{3.18}$$

$$y_m(t) = -\cos(\theta_r)L_2 + t\sin(\theta_r)L_2\sqrt{-2K(\cos(\theta_r) - \cos(\theta_0))} - \frac{1}{2}gt^2 \tag{3.19}$$

$$\tag{3.20}$$

Now that we know the trajectory of the projectile we are interested in the range of the seesaw. We can calculate the range by first finding the time at which the projectile hits the ground. Solving for $y_m(t) = -H$ gives us this time, t_h, assuming we fire on a flat terrain. We can then find the range of the seesaw, namely $s = x_m(t_h)$.

Other than the trajectory and the range of the projectile we also want to find the movement of the seesaw during phase III for completion and possible further research. This movement will be different from phase II since the mass of the projectile no longer contributes to the Lagrangian. We will therefore have to find the new Lagrangian similar to how we did in section 3.1.

$$\mathscr{L} = T - U = \frac{1}{2}\dot{\theta}^2\left(M(L_1 + L_M)^2 + I_b\right) - g\cos(\theta)\left(M(L_1 + L_M) - m_b L_b\right) \tag{3.21}$$

Notice that the terms related to the projectile have indeed vanished when comparing it to equation 3.8. When we insert equation 3.21 into equation 3.9 we obtain

$$\ddot{\theta} = K' \sin(\theta) \tag{3.22}$$

with

$$K' = g\frac{M(L_1 + L_M) - m_b L_b}{M(L_1 + L_M)^2 + I_b}$$

As we can see when comparing this to equation 3.10 we have the same ODE but with a different factor. Therefore, the solution will also be given by

$$\frac{1}{2}\dot{\theta}^2 = -K'\cos(\theta) + \tau' \tag{3.23}$$

with τ' some constant. Using equation 3.14 we see that at $t = t_r$, $\dot{\theta} = \dot{\theta}_r = \sqrt{-2K(\cos(\theta_r) - \cos(\theta_0))}$. Thus, we find $\tau' = K'\cos(\theta_r) + \frac{1}{2}\dot{\theta}_r^2$. When further writing out τ' we get

$$\tau' = (K' - K)\cos(\theta_r) + K\cos(\theta_0) \tag{3.24}$$

$$= \tau + (K' - K)\cos(\theta_r) \tag{3.25}$$

As a consequence, when $m \ll M$ we see that $K' - K$ will be small and thus the change in the movement of the seesaw compared with phase II will be small as well. Filling the found value of τ' into equation 3.23 gives us the exact solution for $\dot{\theta}$ as a function of θ.

$$\dot{\theta} = \pm\sqrt{-2K'(\cos(\theta) - \cos(\theta_r)) + \dot{\theta}_r^2} \tag{3.26}$$

Note that here the positive and negative functions alternate as we now have that the seesaw starts oscillating back and forth. Therefore, the speed is sometimes positive and sometimes negative. We can write this as

$$\dot{\theta} = (-1)^n\sqrt{-2K'(\cos(\theta) - \cos(\theta_r)) + \dot{\theta}_r^2} \tag{3.27}$$

where n is the number of times $\dot{\theta}$ has been zero other than the initial condition.

4

Mangonel

We will now apply the theory of section 2.1 to the mangonel. The results of which can be found in section 6.2. Again, we will look at the mangonel and try to understand it intuitively before going into the mathematics behind it. Afterwards, we will redefine the coordinates of the projectile and formulate the Lagrangian. By making use of the Euler-Lagrange equation we can then find the ODEs for the angles. As discussed in section 1.1.2 the shooting process of the mangonel can be divided into three phases. Therefore, we will analyse these three different phases separately. Phase I will be discussed in section 4.1 and phases II and III will be discussed in sections 4.2 and 4.3 respectively.

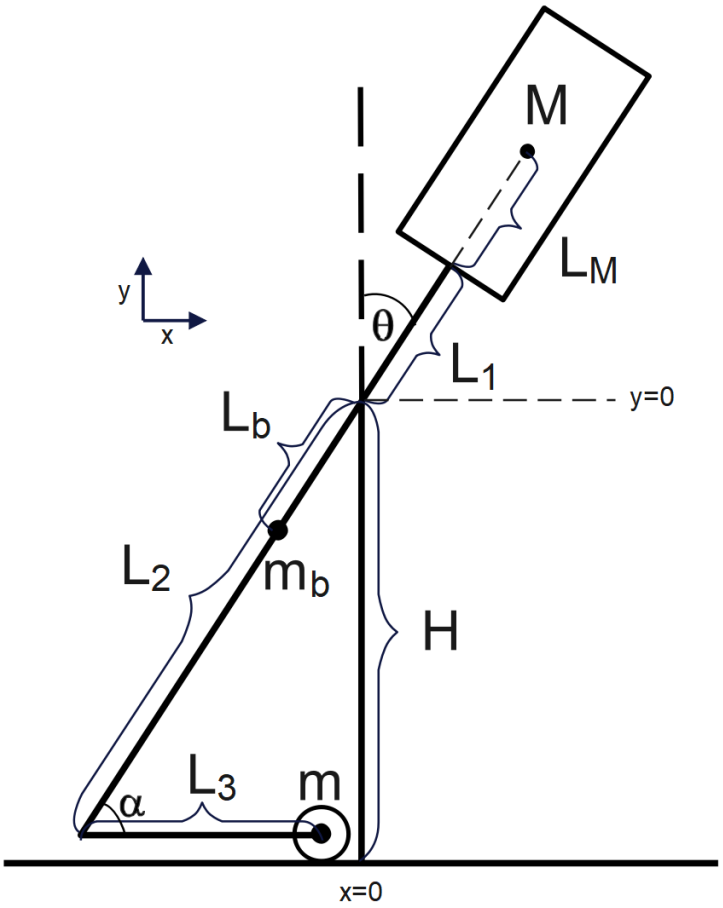

Figure 4.1: Schematic representation of the mangonel with all the variables defined as in table 1.1. The main beam rotates around the origin while the rope can rotate around its anchor point. As we can see all the coordinates can be expressed using θ and α since all the lengths are fixed. θ and α are the only variables dependent on time while all other variables are fixed constants.

Let us first look at the schematics of the mangonel and try to understand what is happening intuitively. When looking at figure 4.1 we see it is very similar to the seesaw. The only difference is that the projectile is now connected to the main beam by means of a rope which we assume to be massless and always fully extended. This essentially means we model the rope as a beam. Throughout, this paper we will keep on using the term rope but it is important to remember that the rope is not flexible. This causes the system to need an extra coordinate in order to fully describe it. We will use the angle α to do this, which is the angle between the main beam and the rope. From figure 4.1 we can also see that the coordinates for the centre of mass of the beam and the counterweight are the same as in chapter 3. And that only the coordinates of the projectile have changed. They should be the coordinates of the projectile for the seesaw (equation 3.2) with some deviation due to the rope which is dependent on α.

Also, note that we can again see the different phases come into play. During phase I the projectile is in the trough on the ground and we need to make use of the theory of section 2.1.2 in order to take this constraint into account. During phase II the projectile has been lifted off the ground and we can, therefore, get rid of the constraint from phase I. Lastly, once the release condition has been met we move into phase III. In this phase, the rope can be neglected as we assume it to be massless. This reduces the problem to the same as for the seesaw in phase III which we discussed in section 3.2.

Now that we have looked at the mangonel's schematic we can continue with finding the coordinates of the projectile. We refer to figure 4.1 to see how the angles, masses and lengths are defined. By making use of trigonometry principles we obtain that

$$\begin{cases} x_m = -\sin(\theta)L_2 + \sin(\alpha+\theta)L_3 \quad \Longrightarrow \quad \dot{x}_m = -\dot{\theta}\cos(\theta)L_2 + (\dot{\alpha}+\dot{\theta})\cos(\alpha+\theta)L_3 \\ y_m = -\cos(\theta)L_2 + \cos(\alpha+\theta)L_3 \quad \Longrightarrow \quad \dot{y}_m = \dot{\theta}\sin(\theta)L_2 - (\dot{\alpha}+\dot{\theta})\sin(\alpha+\theta)L_3 \end{cases} \tag{4.1}$$

Note that this is indeed similar to the equation 3.2 but with some deviation added due to the rope. Other than the coordinates we also need to have the initial conditions. We use the initial conditions for θ and α and the release angle α_r as defined in table 1.1.

4.1. Phase I

In phase I the projectile is moving through the trough which we assume is on the ground and parallel to it. Therefore $y_m = -H$ in this phase. We can write this as a holonomic constraint

$$f(\theta,\alpha) = H - \cos(\theta)L_2 + \cos(\alpha+\theta)L_3 = 0 \tag{4.2}$$

As discussed in section 2.1.2 we can incorporate this constraint into our calculations through the use of the Lagrangian multiplier. By using this method we get for all coordinates q_i

$$\frac{d}{dt}\frac{\delta\mathscr{L}}{\delta\dot{q}_i} - \frac{\delta\mathscr{L}}{\delta q_i} - \lambda(t)\frac{\delta f}{\delta q_i} = 0 \tag{4.3}$$

Before being able to calculate the Lagrangian we must first calculate the kinetic and potential energy. Similar as to what we did in section 3.1 we can substitute the coordinates and their time derivatives into equations 3.4 and 3.6 to get our energies. We can then obtain our Lagrangian by subtracting the potential energy from the kinetic energy. This gives us

$$\begin{aligned} \mathscr{L} = T - U = \frac{1}{2}\dot{\theta}^2\left(M(L_1+L_M)^2 + I_b + m(L_2^2+L_3^2) - 2m\cos(\alpha)L_2L_3\right) + \frac{1}{2}\dot{\alpha}^2 mL_3^2 \\ +\dot{\alpha}\dot{\theta}m(L_3^2 - \cos(\alpha)L_2L_3) - g\cos(\theta)\left(M(L_1+L_M) - m_bL_b - mL_2\right) - g\cos(\alpha+\theta)mL_3 \end{aligned} \tag{4.4}$$

Now that we have found our Lagrangian we can substitute equation 4.4 into equation 4.3 with f as described earlier. This will give us the coupled ODEs for the two coordinates θ and α. They are given by

$$\begin{aligned} \ddot{\theta}\left(M(L_1+L_M)^2 + I_b + m(L_2^2+L_3^2) - 2m\cos(\alpha)L_2L_3\right) + \ddot{\alpha}(mL_3^2 - \cos(\alpha)mL_2L_3) + \dot{\alpha}^2\sin(\alpha)mL_2L_3 \\ +2m\dot{\alpha}\dot{\theta}\sin(\alpha)L_2L_3 = \sin(\theta)\left(gM(L_1+L_M) - gm_bL_b - gmL_2 + \lambda L_2\right) + \sin(\alpha+\theta)(mgL_3 - \lambda L_3) \end{aligned} \tag{4.5}$$

$$\ddot{\alpha}mL_3^2 + \ddot{\theta}m(L_3^2 - cos(\alpha)L_2L_3) = \dot{\theta}^2 m\sin(\alpha)L_2L_3 + \sin(\alpha+\theta)(mgL_3 - \lambda L_3) \tag{4.6}$$

For simplicity we can write these equations as follows

$$\ddot{\theta} a_{11}(\alpha) + \ddot{\alpha} a_{12}(\alpha) + \lambda a_{13}(\theta, \alpha) = b_1(\alpha, \theta, \dot{\alpha}, \dot{\theta}) \tag{4.7}$$

$$\ddot{\alpha} a_{22} + \ddot{\theta} a_{21}(\alpha) + \lambda a_{23}(\alpha, \theta) = b_2(\alpha, \theta, \dot{\theta}) \tag{4.8}$$

with a_{ij} and b_i terms that do not depend on $\ddot{\theta}$, $\ddot{\alpha}$ or λ. To see the exact terms we refer to the appendix.

We now have two equations (4.7 and 4.8) with three unknowns, namely $\theta(t)$, $\alpha(t)$, and $\lambda(t)$. We cannot solve this with only two equations. However, as we also discussed in section 2.1.2 we can make use of the constraint itself to obtain three equations with three unknowns which is generally solvable. Rather than just taking the constraint itself we differentiate equation 4.2 twice so that we also get terms with $\ddot{\theta}$ and $\ddot{\alpha}$. It will become apparent why we will need this in a moment. The second time derivative of equation 4.2 is given by

$$\ddot{f} = \ddot{\theta} \sin(\theta)\, L_2 + \dot{\theta}^2 \cos(\theta)\, L_2 - \left(\ddot{\alpha} + \ddot{\theta}\right) \sin(\alpha + \theta)\, L_3 - \left(\dot{\alpha} + \dot{\theta}\right)^2 \cos(\alpha + \theta)\, L_3 = 0 \tag{4.9}$$

Where we know this is equal to zero since f itself is equal to zero for all times during phase I.

We can now write equation 4.9 like equations 4.7 and 4.8.

$$\ddot{\theta} a_{31}(\alpha) + \ddot{\alpha} a_{32}(\alpha) + \lambda a_{33} = b_3(\alpha, \theta, \dot{\alpha}, \dot{\theta}) \tag{4.10}$$

with again a_{ij} and b_i independent of $\ddot{\theta}$, $\ddot{\alpha}$ and λ. We now have three equations each of which can be written in the same manner but with different factors. Therefore, we can write this using matrix representation. The matrix equation for equations 4.7, 4.8, 4.10 is the following.

$$\begin{pmatrix} a_{11} & a_{12} & a_{13} \\ a_{21} & a_{22} & a_{23} \\ a_{31} & a_{32} & a_{33} \end{pmatrix} \begin{pmatrix} \ddot{\theta} \\ \ddot{\alpha} \\ \lambda \end{pmatrix} = \begin{pmatrix} b_1 \\ b_2 \\ b_3 \end{pmatrix} \tag{4.11}$$

$$A \begin{pmatrix} \ddot{\theta} \\ \ddot{\alpha} \\ \lambda \end{pmatrix} = \vec{b}$$

Since we have the matrix representation of all the coupled ODEs we can find the exact formulas for $\ddot{\theta}$, $\ddot{\alpha}$, and λ as a function of $\dot{\theta}, \dot{\alpha}, \theta$, and α by multiplying the equation with the inverse of A if it exists. This inverse exists as long as the determinant of A is unequal to zero. It is now evident that we had to take the second order time derivative of equation 4.2 since otherwise we would have had $a_{31} = a_{32} = a_{33} = 0$ which would always results in the determinant being equal to zero. This would have resulted in us being unable to find the formulas for $\ddot{\theta}$, $\ddot{\alpha}$, and λ. In the appendix we will prove that the inverse of this matrix does indeed exist. So, by multiplying equation 4.11 with the inverse of A we get

$$\begin{pmatrix} \ddot{\theta} \\ \ddot{\alpha} \\ \lambda \end{pmatrix} = A^{-1} \vec{b} \tag{4.12}$$

This gives us the formulas we need so that we can simulate the motion of the mangonel by solving numerically to obtain $\theta(t)$ and $\alpha(t)$.

4.2. Phase II

Now that we have found the formulas for phase I we need to know when we transition to phase II. We know we transition to phase II when the projectile comes off the ground. This happens when the magnitude of the gravitational force on the projectile is equal and opposite to the magnitude of the constraint force parallel to the y-axis. We can calculate the constraint force parallel to the q_i-axis using the theory discussed in section 2.1.2. There we found that the force parallel to the q_i-axis due to the constraint was given by

$$F_{q_i} = -\lambda \frac{\delta f}{\delta q_i} \tag{4.13}$$

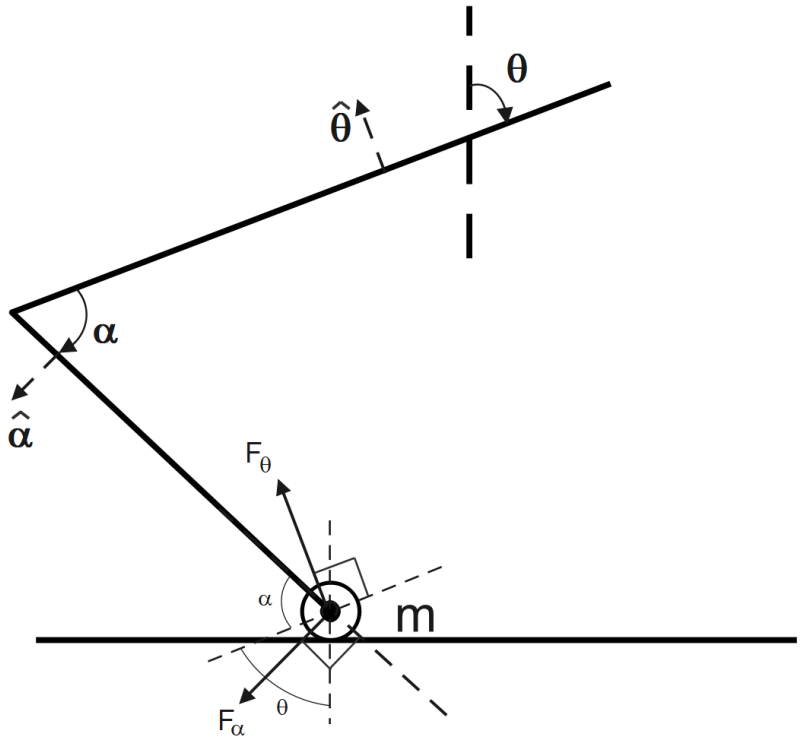

Figure 4.2: In this figure the direction of the θ and α axis are defined by $\hat{\theta}$ and $\hat{\alpha}$ respectively. An example of a possible constraint force is also shown. Note that the angle between the forces is given by α and that the angle between the vertical and the slanted dashed line is given by θ. These two angles are needed in order to get to equation 4.16

So we can decompose the constraint force in two, one in the θ-direction and one in the α-direction. See figure 4.2 for how these directions are defined.

$$F_\theta = -\lambda \frac{\delta f}{\delta \theta} = -\lambda(\sin(\theta)\, L_2 - \sin(\alpha+\theta)\, L_3) \tag{4.14}$$

$$F_\alpha = -\lambda \frac{\delta f}{\delta \alpha} = \lambda \sin(\alpha+\theta)\, L_3 \tag{4.15}$$

Therefore, the constraint force parallel to the y-axis is equal to

$$F_y = \sin(\theta)F_\theta - \sin(\alpha+\theta)F_\alpha = -\lambda(\sin(\theta)^2 L_2 - \sin(\alpha+\theta)\sin(\theta)L_3 + \sin(\alpha+\theta)^2 L_3) \tag{4.16}$$

which is obtained by applying trigonometry to figure 4.2.

Now that we have found the constraint force parallel to the y-axis we know that the projectile becomes airborne as soon as this force is equal and opposite to the gravitational force $-mg$. Once this is the case we can drop the constraint. We do this by choosing $\lambda(t) = 0$ as this reduces equation 4.3 back to the original Euler-Lagrange equation. Since $\lambda(t) = 0$ equation 4.11 simplifies to

$$\begin{pmatrix} a_{11} & a_{12} \\ a_{21} & a_{22} \end{pmatrix} \begin{pmatrix} \ddot{\theta} \\ \ddot{\alpha} \end{pmatrix} = \begin{pmatrix} b_1 \\ b_2 \end{pmatrix} \tag{4.17}$$

with a_{ij} and b_i the same as in phase I. This makes it possible for us to find the formulas for $\ddot{\theta}$ and $\ddot{\alpha}$ on the condition that A has an inverse. We will again show that its inverse exists in the appendix.

4.3. Phase III

We have now found the motion of the seesaw up and till the moment the projectile is fired. We know the projectile is released, and therefore we move into phase III, as soon as $\alpha = \alpha_r$. From this moment on, we can ignore the rope completely as we assumed it to be massless. Therefore, the solutions for the mangonel of phase III are the same as the solutions for the seesaw. We discussed this in section 3.2.

We are also interested in the motion of the projectile after it has been released. Using equation 4.1 and using $\theta = \theta_r$ and $\alpha = \alpha_r$, where θ_r is the value for θ when the projectile is released, we get the coordinates and the speed of the projectile at the time of release.

Just like for the seesaw we assume there to be no air resistance and thus $\ddot{x} = 0$ and $\ddot{y} = -g$. Therefore, the trajectory of the projectile after its release is given by

$$x_m(t) = -\sin(\theta_r)L_2 + \sin(\alpha_r + \theta_r)L_3 + t\left(-\dot{\theta}_r \cos(\theta_r)L_2 + (\dot{\alpha}_r + \dot{\theta}_r)\cos(\alpha_r + \theta_r)L_3\right) \tag{4.18}$$

$$y_m(t) = -\cos(\theta_r)L_2 + \cos(\alpha_r + \theta_r)L_3 + t\left(\dot{\theta}_r \sin(\theta_r)L_2 - (\dot{\alpha}_r + \dot{\theta}_r)\sin(\alpha_r + \theta_r)L_3\right) - \frac{1}{2}gt^2 \tag{4.19}$$

where $\theta_r, \alpha_r, \dot{\theta}_r, \dot{\alpha}_r$ represent the corresponding values at the moment of release. In order to obtain the range of the mangonel we can again solve for $y_m = -H$. This gives us the time the object hits the ground, t_h. The range is then given by $s = x_m(t_h)$

5

Trebuchet

We have now treated the seesaw and mangonel in the previous chapters. In this chapter, we will apply the theory from section 2.1 to the trebuchet. The results of the model described in this chapter can be found in section 6.3. The trebuchet differs from the mangonel by the way the counterweight is attached to the main beam. The steps taken are very similar to the ones in chapter 4 where we discussed the mangonel. For that reason, we will not explain every step very extensively but refer to the appendix where the calculations are done in full as well as chapter 4 where the same steps are taken with more explanation.

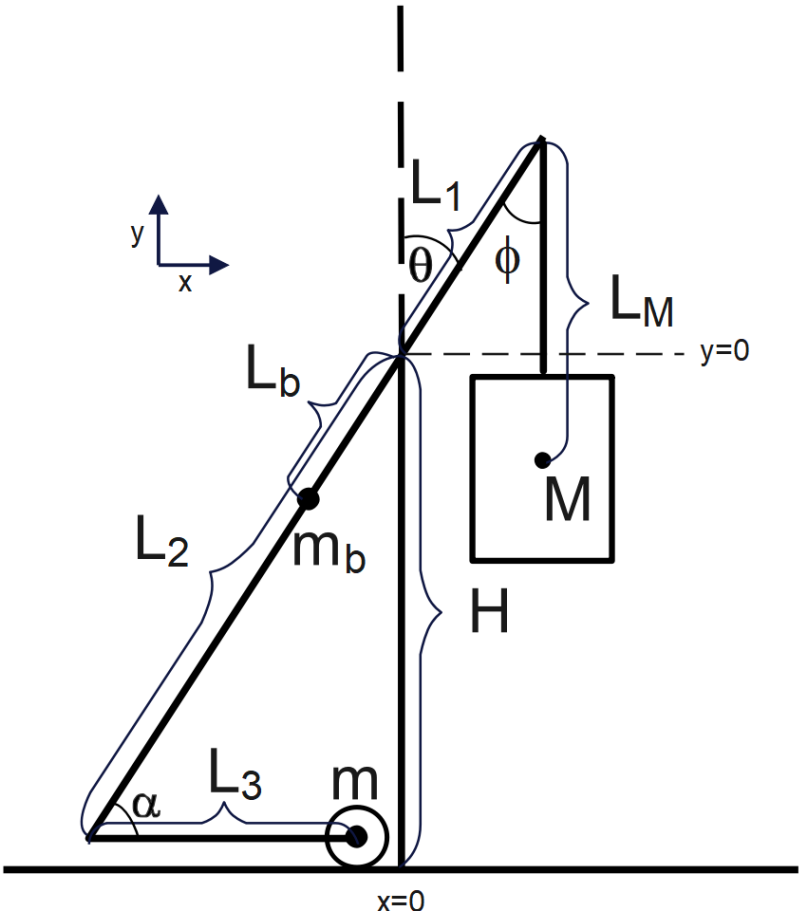

Figure 5.1: Schematic representation of the trebuchet. With all the variables defined as in table 1.1.

Before discussing the mathematics let us first look at the trebuchet itself and its important aspects. The schematics of the trebuchet are shown in figure 5.1. Much like the mangonel, the projectile is also attached to the main beam by means of a rope which we assume to be rigid. However, the counterweight is no longer directly attached to the beam but hangs from the main beam. Note that the counterweight is attached by a beam and not a rope like the projectile is. Since we now have another hinge we also need another angle to fully define the system. For this, we will use the angle ϕ. As another consequence of this extra hinge, the coordinates of the counterweight have also changed compared to the seesaw and mangonel.

We can now start by calculating the new coordinates of the counterweight. We refer to figure 5.1 for the angles, masses and lengths involved. Using trigonometry principles we get

$$\begin{cases} x_M = \sin(\theta)L_1 + \sin(\phi-\theta)L_M \Longrightarrow \dot{x}_M = \dot{\theta}\cos(\theta)\,L_1 + \left(\dot{\phi}-\dot{\theta}\right)\cos\left(\phi-\theta\right)L_M \\ y_M = \cos(\theta)L_1 - \cos(\phi-\theta)L_M \Longrightarrow \dot{y}_M = -\dot{\theta}\sin(\theta)\,L_1 + \left(\dot{\phi}-\dot{\theta}\right)\sin\left(\phi-\theta\right)L_M \end{cases} \tag{5.1}$$

We use the initial conditions for θ, α, and ϕ and the release angle α_r as defined in table 1.1

5.1. Phase I

During phase I we need, just like for the mangonel, to ensure that the projectile does not go below the ground. We again do this by making use of the theory from section 2.1.2. Since the coordinates of the projectile are the same as for the mangonel we can use the same constraint as we introduced in equation 4.2. Using a similar approach as we did for the mangonel we can calculate the kinetic and potential energy, and with that the lagrangian. If we again use equation 4.3 for the different coordinates we get a total of three equations, one for all the three angles. Combining this again with the twice differentiated constraint we can write the problem as a matrix equation. The complete calculations for all these steps can be found in the appendix.

$$\begin{pmatrix} a_{11} & a_{12} & a_{13} & a_{14} \\ a_{21} & a_{22} & a_{23} & a_{24} \\ a_{31} & a_{32} & a_{33} & a_{34} \\ a_{41} & a_{42} & a_{43} & a_{44} \end{pmatrix} \begin{pmatrix} \ddot{\theta} \\ \ddot{\alpha} \\ \ddot{\phi} \\ \lambda \end{pmatrix} = \begin{pmatrix} b_1 \\ b_2 \\ b_3 \\ b_4 \end{pmatrix} \tag{5.2}$$

$$A \begin{pmatrix} \ddot{\theta} \\ \ddot{\alpha} \\ \ddot{\phi} \\ \lambda \end{pmatrix} = \overrightarrow{b}$$

where again a_{ij} and b_i are independent of $\ddot{\theta}$, $\ddot{\alpha}$, $\ddot{\phi}$, and λ. We can get the formulas for $\ddot{\theta}, \ddot{\alpha}, \ddot{\phi}$, and λ by multiplying equation 5.2 with the inverse of A if it exists. The existence of the inverse of A is proved in the appendix. After we have found the formulas we can solve for $\theta(t)$, $\alpha(t)$ and $\phi(t)$ numerically.

5.2. Phase II

Just like for the mangonel we know that we move to phase II when the gravitational force on the projectile is canceled out by the tension in the rope. Since the constraint itself is the same so is the equation for the constraint force. So similar as for the mangonel when equation 4.16 is equal and opposite to the gravitational force mg we drop the constraint which simplifies equation 5.2 to

$$\begin{pmatrix} a_{11} & a_{12} & a_{13} \\ a_{21} & a_{22} & a_{23} \\ a_{31} & a_{32} & a_{33} \end{pmatrix} \begin{pmatrix} \ddot{\theta} \\ \ddot{\alpha} \\ \ddot{\phi} \end{pmatrix} = \begin{pmatrix} b_1 \\ b_2 \\ b_3 \end{pmatrix} \tag{5.3}$$

with a_{ij} and b_i the same as in phase I. We can again multiply equation 5.3 with the inverse of the matrix, as long as it exists, to get the formulas for $\ddot{\alpha}$, and $\ddot{\phi}$. After which we can numerically solve the ODEs. The existence of the inverse is again proved in the appendix.

5.3. Phase III

Once the release condition has been met we move into phase III. In phase III we, just like with the mangonel, can ignore the rope since the projectile is detached from the trebuchet and we assume the rope to be massless.

Therefore, we can simplify the matrix representation as follows.

$$\begin{pmatrix} a_{11} & a_{13} \\ a_{31} & a_{33} \end{pmatrix} \begin{pmatrix} \ddot{\theta} \\ \ddot{\phi} \end{pmatrix} = \begin{pmatrix} b_1 \\ b_3 \end{pmatrix} \tag{5.4}$$

with a_{ij} and b_i the same as in phase I albeit with $m = 0$ to account for the fact that the projectile is now detached. It is important to note that we cannot use equation 5.3 with $m = 0$ as this would result in a matrix A that has no inverse. Therefore, it is needed to simplify the matrix into this form. We can again find $\theta(t)$ and $\phi(t)$ by multiplying equation 5.4 with the inverse of the matrix and solving numerically.

The last thing that remains is the trajectory of the projectile. Due to the fact that the coordinates of the projectile are the same as for the mangonel the motion is also the same and is thus described in equations 4.18 and 4.19.

6

Results

In this chapter, we will look at the motions of the different catapults as well as their range. The maximum bending moment and the corresponding thickness needed for the beam will be discussed in chapter 7.

6.1. Seesaw

For the seesaw, we start by comparing the algebraic solution for $\dot{\theta}$ with the solution found by applying the forward Euler method on $\ddot{\theta}$. After which we will look at the movement of the seesaw itself and how these movements change throughout the phases. Lastly, we will look at the trajectory of the projectile and what its range is depending on the release angle.

In chapter 3 we saw that we could find exact algebraic solutions for $\dot{\theta}$ in phases II and III. These solution were described in equations 3.14 and 3.26. Therefore, we can first take a look at the exact solution of the angular velocity compared to the angular velocity obtained by applying the forward Euler method to equation 3.10.

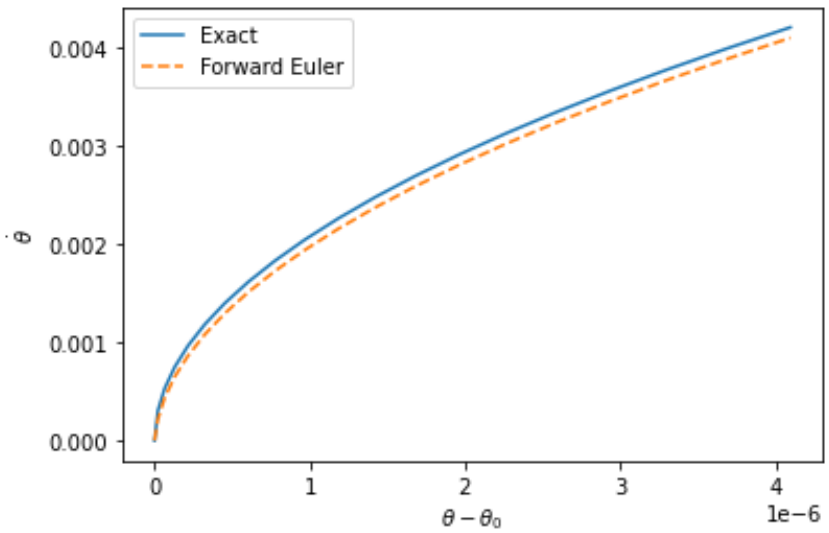

Figure 6.1: The algebraic and numerical solutions for $\dot{\theta}$ for the first 20 time steps. As can be seen the two solutions differ slightly but the difference stays within the numerical accuracy. Here we used $\theta_r = 0.86\pi$.

The intermediate analytical (3.14) and numerical solutions for $\dot{\theta}$ of the first 20 time steps (0.002 s) are shown in figure 6.1. We can see that the solutions both start at $\dot{\theta} = 0$ which is in line with the initial condition. We then see that the exact solution increases faster than the numerical one. However, when we look further we see that the difference between the two graphs remains constant. The two graphs are the same within the numerical accuracy. We can, therefore, assume the numerical solution to be accurate given the numerical accuracy.

Now that we have established that the forward Euler method results in an accurate solution we can further analyse this system. We continue by looking at the motion of the seesaw which is described by θ and its derivative.

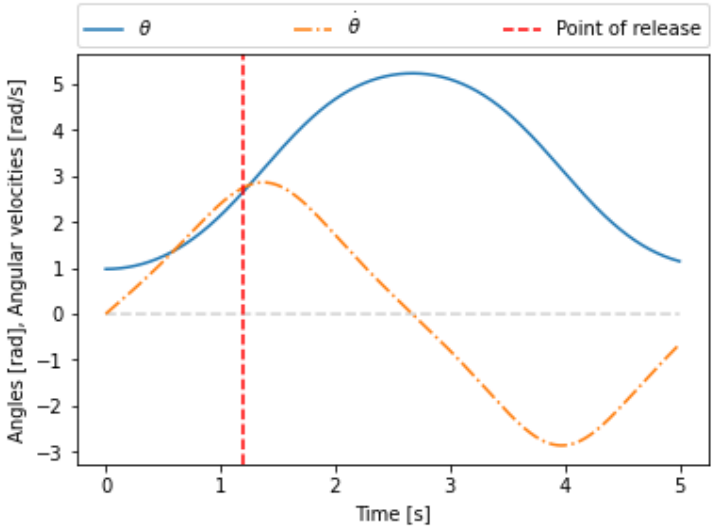

Figure 6.2: θ and $\dot{\theta}$ for the seesaw with $\theta_r = 0.86 \times \pi$ against the time. The point of release is shown by the vertical dashed red line.

In figure 6.2 we see the angle θ and its corresponding angular velocity. We see that θ depicts a sinusoid which is not very surprising when we take a step back and realize we are essentially looking at a seesaw rocking back and forth. Moreover, we could possibly expect the slope of the graphs to change after the point of the release. However, the shape of both graphs is very similar both before and after the release. This is mostly due to the fact that the projectile is light compared to the counterweight and thus its contribution is minimal. When we look at equation 3.25 we see that the angular velocity has a constant term dependent on $K' - K$ which becomes larger when the projectile is heavier. Therefore, if we increase the weight of the projectile to 200 kg we expect to see a significant change in the slopes of the graphs after the point of release. This can be seen in figure 6.3.

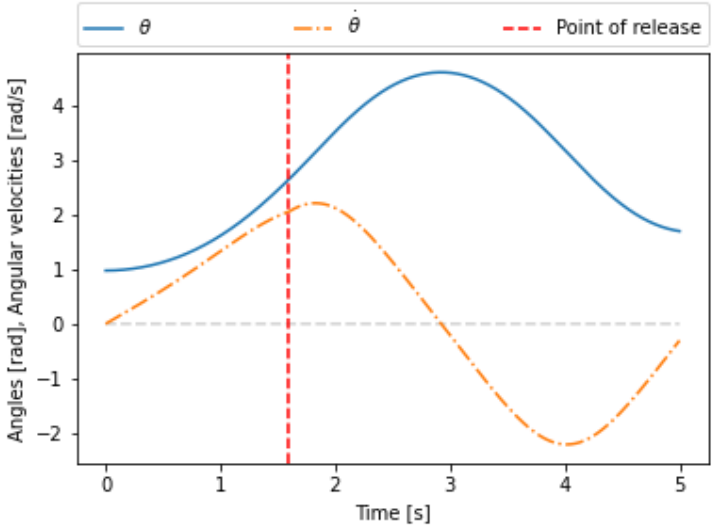

Figure 6.3: θ and $\dot{\theta}$ for the seesaw with $\theta_r = 0.86 \times \pi$ against the time. Here $m = 200$kg. The point of release is shown by the vertical dashed red line.

Indeed we see that the slope of $\dot{\theta}$ changes after the point of release more clearly than in figure 6.2. Additionally, we see that θ does not become as large as in figure 6.2 and also does not return to or near its initial

value. This is due to the fact that the mass of the projectile was very high and, therefore, after the release, a lot of energy is lost from the system.

Now that we have taken a look at the movement of the seesaw we can look at the projectile and its range. The typical trajectory followed by the projectile is shown in figure 6.4.

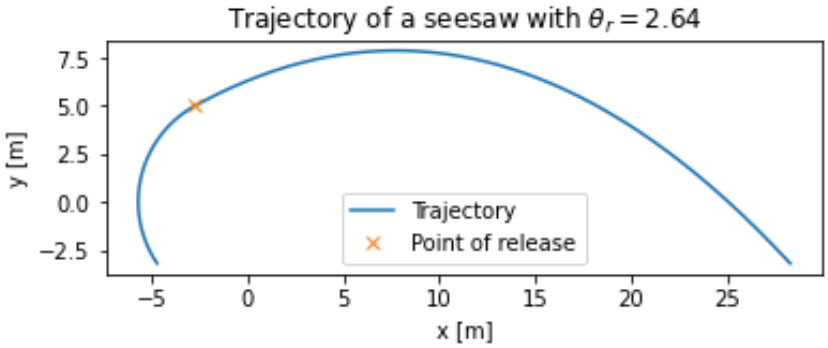

Figure 6.4: The trajectory followed by the projectile of a seesaw with $\theta_r = 0.84 \times \pi$. Note that the projectile starts off with a circular motion as it is still attached to the seesaw. After the point of release, the projectile is detached from the seesaw and follows a parabolic trajectory since we assume there to be no air resistance.

As we can see the projectile starts off with a circular motion which is logical as it is rotating around the pivot point at a fixed distance. After the release, the projectile moves on with a parabolic trajectory as we described in section 3.2. Moreover, we might be interested in the maximum range of a given seesaw. We can calculate the range for different values of θ_r which is shown in figure 6.5. This gives us the maximum range of 28.3m for $\theta_r = 2.675$ rad.

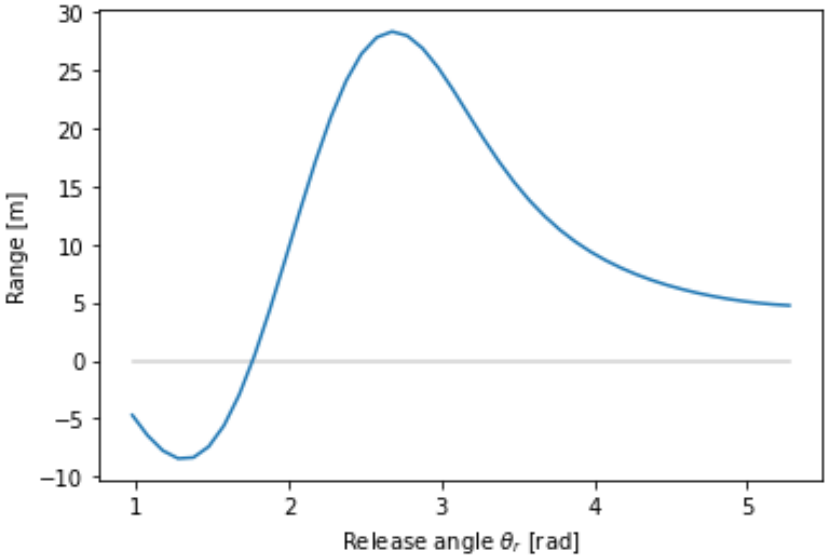

Figure 6.5: The range of the seesaw for different values of θ_r. We see a maximal range for $\theta_r = 2.675$.

6.2. Mangonel

For the mangonel, we will look at the movement of the mangonel and how this changes throughout the different phases. Next, we will look at the trajectory of the projectile and the range depending on the release angle α_r. Since we have not found an exact solution for $\dot{\theta}$ or θ in chapter 4 we cannot compare the numerical results with an algebraic solution. However, as we saw in section 6.1 we know that for the seesaw the forward Euler method is accurate within the numerical accuracy and the error does not grow as the system develops further in time. We will assume the same holds for the mangonel and later for the trebuchet as well. We will come back to the possible consequences of this assumption in the discussion in chapter 8.

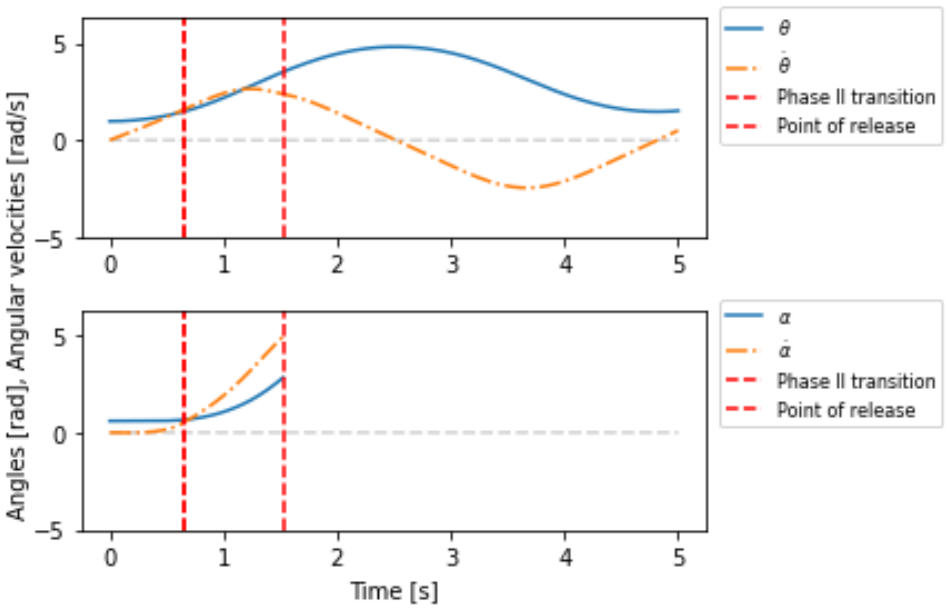

Figure 6.6: θ, $\dot{\theta}$, α and $\dot{\alpha}$ for the mangonel with $\alpha_r = 0.9 \times \pi$ against the time. The transition to phase II is indicated by the first vertical dashed red line and the point of release is shown by the second vertical dashed red line.

In figure 6.6 the angles and their corresponding angular velocities are shown. As can be seen the angle α and its angular velocity are dropped after the point of release since the rope is assumed to be massless as discussed in section 4.3. Moreover, we can see that $\dot{\alpha}$ quickly becomes larger than $\dot{\theta}$ and also increases much more rapidly. This is what we expected as the rope introduces a whiplike movement which greatly accelerates the projectile which in turn heavily increases the maximum range. Lastly, we may also note that θ and $\dot{\theta}$ are very quite similar to the case of the seesaw in figure 6.2. This is again due to the fact that the mass of the projectile is very small compared to the counterweight and, therefore, the change in the projectile's coordinates has little effect on θ and $\dot{\theta}$.

We have now looked at the movement of the mangonel described by θ, α and their derivatives and can, therefore, move on to the trajectory and range of the projectile. Let us first look at figure 6.7 where we plot the range of the mangonel for different values of α_r. The maximum range of 196.1m is obtained for a release angle of 2.196 rad.

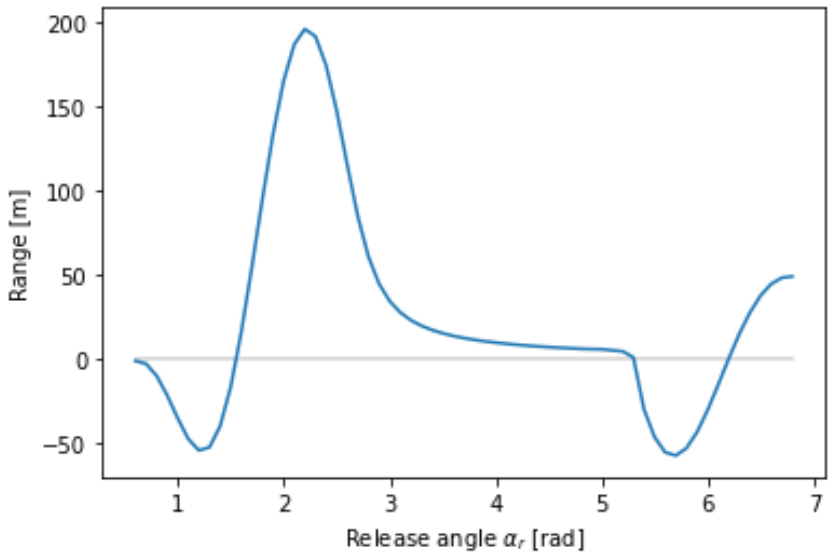

Figure 6.7: The range of the mangonel for different values of α_r.

When comparing this figure to figure 6.5 we first notice that the range has increased roughly sixfold. This indeed displays the whiplike movement introduced by the rope. Moreover, we can see that there are two ranges of values for α_r where the range of the mangonel becomes negative. Lastly we can also look at the trajectory of the projectile of which a typical example is shown in figure 6.8.

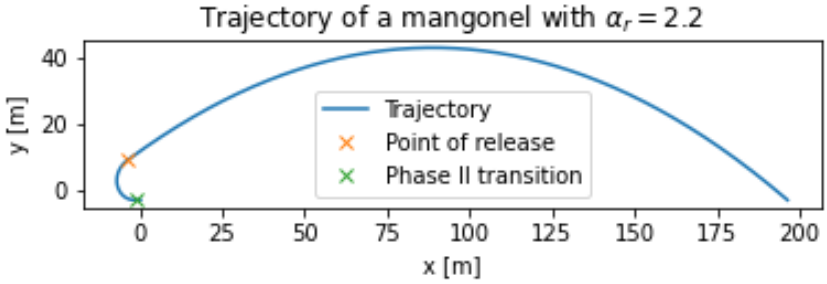

Figure 6.8: The trajectory followed by the projectile of a mangonel with $\theta_r = 2.196$

Surprisingly, the trajectory before phase III looks very similar to that of the seesaw as shown in figure 6.4. We could have expected the projectile to have quite a different trajectory due to the extra pivot introduced by the rope. The trajectory in phase III is the same shape as for the seesaw which makes sense as it is simply a free-falling object. The range is much larger meaning the kinetic energy transferred to the projectile is larger than for the seesaw. And therefore, the efficiency of the mangonel is higher than that of the seesaw.

6.3. Trebuchet

We have now taken a look at the results for both the seesaw and mangonel and will continue with the trebuchet in this section. Like for the mangonel, we will assume the forward Euler method to be accurate for now and come back to this assumption in the appendix. We will start by looking at the angles that describe the movement of the trebuchet. After which we will look at the range of the trebuchet for different release angles and a typical trajectory of the projectile. If we look at the angles over time we obtain figure 6.9.

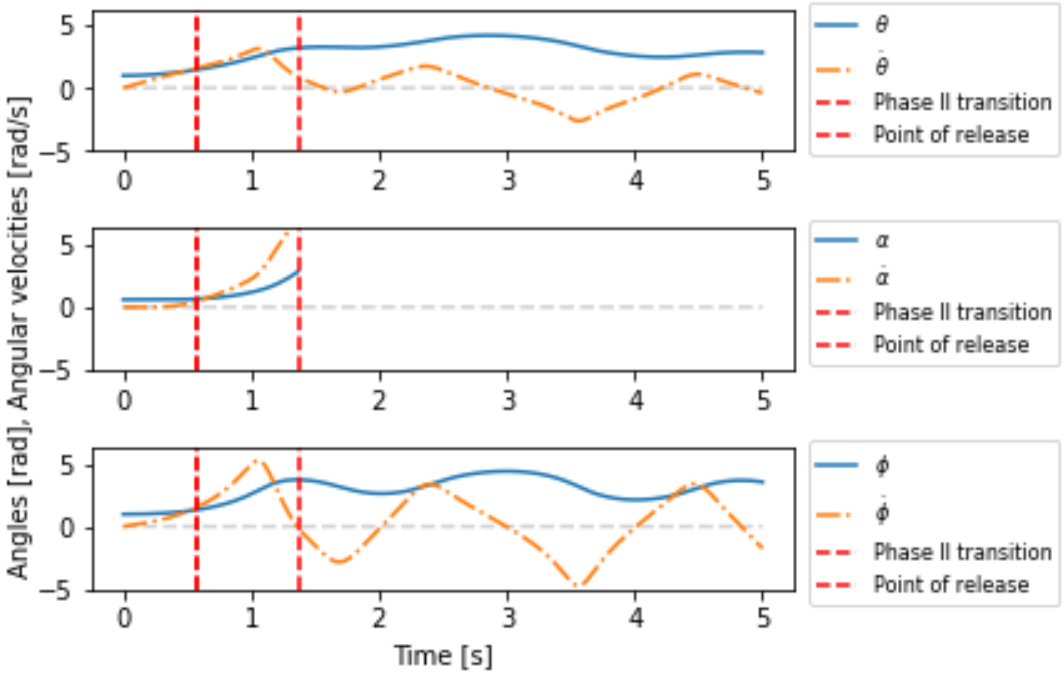

Figure 6.9: $\theta, \dot{\theta}, \alpha, \dot{\alpha}, \phi$ and $\dot{\phi}$ for the trebuchet with $\alpha_r = 0.9 \times \pi$ against the time. The transition to phase II is indicated by the first vertical dashed red line and the point of release is shown by the second vertical dashed red line

As we can see the graph has become far more complex than before. Not only do we have more angles to take into account we can also see how the angles start influencing each other. For example, compared to figure 6.6 we can see that θ is no longer (approximately) described by a sinusoid but has become a rather complex function. Moreover, $\dot{\theta}$ has become more similar to a series of triangular pulses. It is also interesting to note the similarity between θ and ϕ as well as the similarity between their corresponding speeds. This is to be expected since the mass of the counterweight makes up a very big part of the mass of the system. Therefore, it makes sense its movement most greatly influences the overall movement of the system. Lastly, note that the point of release is at a point at which $\dot{\phi} \approx 0$ and $\dot{\theta} \approx 0$ which would mean the beam, as well as the counterweight, are standing nearly still and, therefore, the most kinetic energy is present in the projectile. This makes the trebuchet very efficient compared to the mangonel and the seesaw.

Let us now focus on the maximum range of the trebuchet. Figure 6.10 shows the range for different values of α_r.

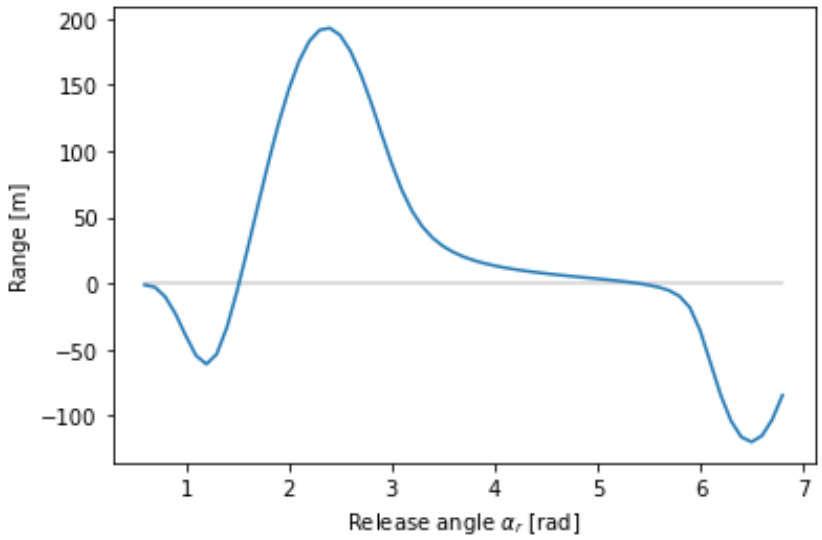

Figure 6.10: The range of the trebuchet for different values of α_r.

Firstly, note that we get a very similar graph as figure 6.7. On closer inspection, we see that the trebuchet has a maximum range of 193.0m for $\alpha_r = 2.396$ rad. When comparing this with the mangonel we find that the trebuchet has a smaller range than the mangonel. This is surprising as we discussed in section 1.1 that the trebuchet was an improvement on the mangonel and we would thus expect the trebuchet to have a larger range than the mangonel. However, perhaps with different lengths of the various beams, a larger range could be obtained. As, after all, this is a complex system where changing one variable also changes the optimum value of other variables it is difficult to find the optimal combination of lengths to get a maximal range.

Let us now also look at an example of a typical trajectory for the trebuchet. This is shown in figure 6.11.

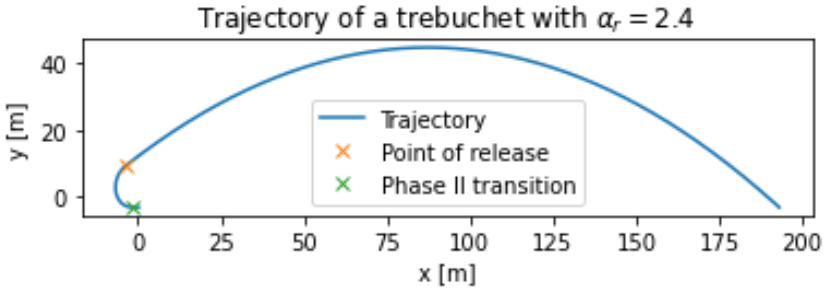

Figure 6.11: The trajectory followed by the projectile of a trebuchet with $\theta_r = 2.396$

This looks remarkably similar to figure 6.8 which is to be expected for such similar ranges and the fact that the coordinates of the projectile have not changed.

7

Bending moment

Now that we have established a way to determine the paths followed by the different catapults and analysed them we can take a look at the internal stresses of the main beam. To do this we will use the theory as described in section 2.2. As discussed there the proper calculations are beyond the scope of this paper. Therefore, we will calculate a lower bound of what the dimensions of the beam would need to be. For all the different catapults we will use the same lower bound based on the seesaw. We do this since the difference in this method between the trebuchets will be small and since this is only a lower bound this difference does not provide much more insight.

For the beam to break we would need that $M_{max} > M_{break}$ where M_{break} was given by equation 2.23. Since we assume the beam to have a width and height of b we get that $M_{break} = \frac{1}{6}\sigma b^3$. Therefore, if at any moment

$$M_{max} > \frac{1}{6}\sigma b^3 \tag{7.1}$$

we known the beam breaks. Moreover, we can calculate the value of b needed to prevent the beam from breaking.

As mentioned, we will only look at the seesaw and assume this lower bound to be equivalent for the mangonel and trebuchet. Before we can calculate the bending moment we need to know the forces acting on the seesaw. They are displayed in figure 7.1.

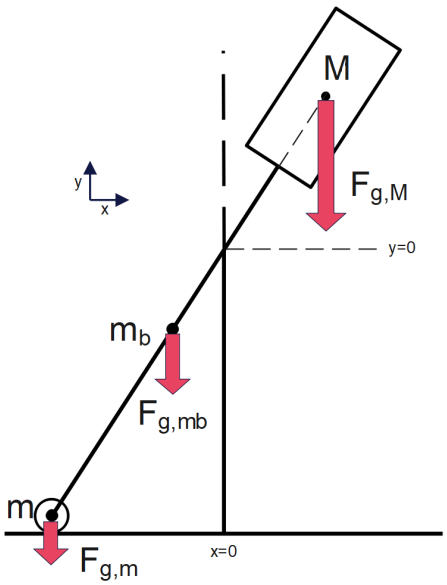

Figure 7.1: The forces acting on the seesaw while shooting that (can) have a component perpendicular to the main beam.

From figure 7.1 we can see that indeed the forces perpendicular to the beam, which play a role in the bending moment, are the greatest when the beam is horizontal. If that is the case the components of the forces perpendicular to the beam would be the same as the forces themselves. Similar to figure 2.1 we can draw the shear moment diagram for the seesaw which is shown in figure 7.2.

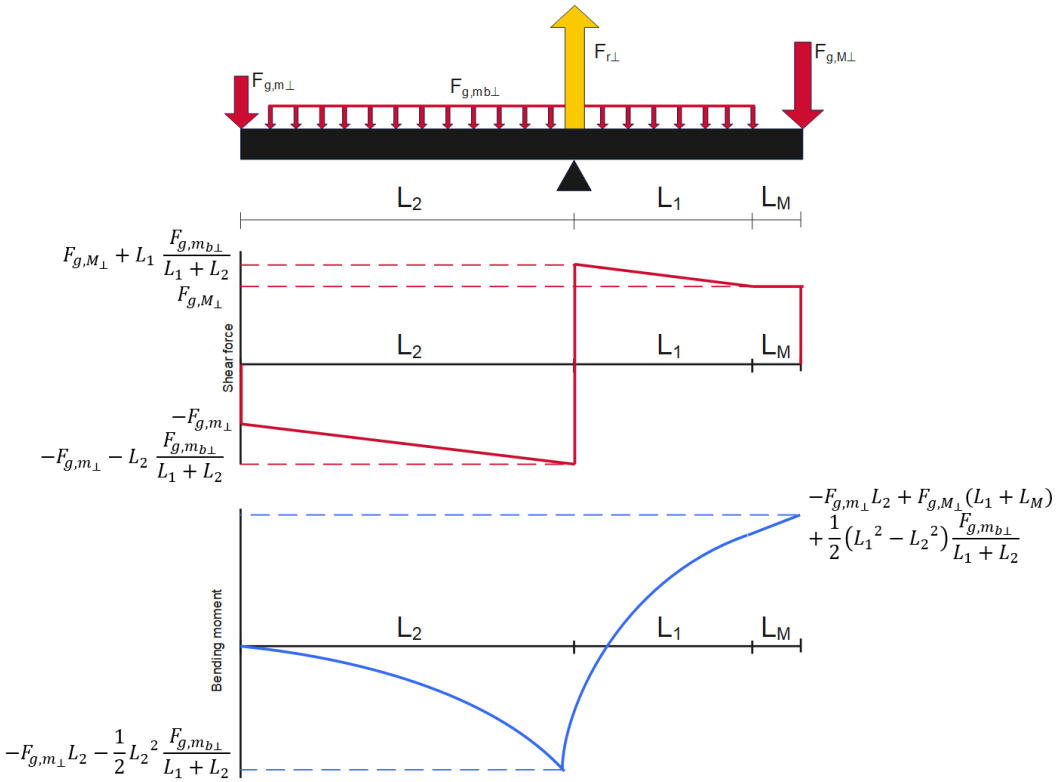

Figure 7.2: The shear moment diagram for the seesaw. In the top picture, the forces perpendicular to the main beam have been drawn. $F_{g,i_\perp}$ represents the gravitational force due to mass i and $F_{r_\perp}$ is the reactive force by the support perpendicular to the beam. The middle picture shows the shear forces on the beam while the bottom figure displays the bending moment on the beam. The moment diagram is obtained by integrating the shear diagram over the length of the beam.

This figure is obtained similar to how we described it in section 2.2 and the full calculations can be found in the appendix. It is important to note that we have two local extrema; one in the origin and one at the centre of mass of the counterweight. One of these extrema, or rather their absolute values, will be the maximum bending moment present in the beam. This maximum bending moment when the beam is horizontal is given by

$$M_{max} = max\left(\left|g\left(M(L_1+L_M) - mL_2 + \frac{1}{2}m_b(L_1-L_2)\right)\right|, \left|g\left(mL_2 + \frac{1}{2}\frac{m_b}{L_1+L_2}L_2^2\right)\right|\right) \tag{7.2}$$

For the values as described in table 1.1 this means $M_{max} = 44$kNm which occurs in the pivot point and not at the counterweight. In order to prevent the beam from breaking we need equation 7.1 not to hold. This is obtained if

$$b = \left(\frac{6M_{max}}{\sigma}\right)^{\frac{1}{3}} \tag{7.3}$$

Using the value for σ from section 2.2 we get that $b = 18.7$ cm. This is a reasonable lower bound for a seesaw with such a heavy counterweight.

8

Discussion

We have discussed three types of trebuchets and have analysed their movements as well as the trajectory and range of their projectiles. In order to do this, we made several assumptions mentioned in section 1.2. In this chapter, we will first put the results found into context and then discuss the consequences of the assumptions made.

The results of all three catapults were presented in chapter 6. In figure 6.1 we compare the obtained solution of the angular velocity for the seesaw with its analytical solution. We see that the error between these two solutions stays within the numerical accuracy. We, therefore, assumed throughout the paper the forward Euler method to give accurate results. However, this assumption could not be true for the mangonel and trebuchet. These catapults are similar to double pendulums as the rope is a pendulum which is attached to the main beam which itself is a pendulum. For the trebuchet, this is the case for the projectile as well as the counterweight. The double pendulum is a well-known chaotic system which means that a small deviation in the initial conditions can induce great changes in how the system develops through time. We, therefore, need to be careful assuming the results of the mangonel and trebuchet to be true. Perhaps due to this small error, the results have changed greatly. Without doing a proper investigation we have not found any sign that this is indeed the case. However, proper research into this subject would be important for the validation of the results. This could be done by looking at a difference in the output induced by a deviation in the initial conditions. If the system is indeed chaotic we would expect large differences to occur due to small deviations in the initial conditions. However, as we discussed in section 1.1 a recently build trebuchet could group its shots within a six-meter square over a distance of 180m. This suggests that the small deviations in the initial conditions that were due to both human and external influences did not create large changes in the results. Therefore, we do not believe we should be very concerned about the possible consequences of the above-named assumption.

We can, however, validate some of the results by comparing them to other studies. For example, [10] and [11] are both studies very similar to ours. Some main differences are that they use different initial conditions and also do not take into account phase I. Therefore, we can only compare the results for the seesaw somewhat properly. If we compare figure 6.5 with their papers we can see that they are very similar. Some small differences might be due to their different initial conditions. Other than this it is hard to compare our results due to the lack of data as well as the lack of dimensions of the machines when data is available.

Another noteworthy observation we made was that the trebuchet had a smaller range than the mangonel which was contrary to what we expected based on section 1.1. As we mentioned in section 6.3 this could be due to the fact that with a different set of lengths the range could be improved significantly. However, we also pointed out that it is difficult to find this optimal set due to the complexity of the system. [12] has tried optimizing the trebuchet. For this, he used a Monte Carlo approach in which random values for several parameters are chosen and in this way, an optimal trebuchet is approached. By using this approach he found a rather optimised trebuchet in his opinion.

In chapter 1 we introduced a few assumptions to simplify the calculations. Firstly, we assumed that air resistance and friction were negligible. Especially, neglecting friction is not accurate as neglecting it results in a trebuchet that would oscillate infinitely. The effect the friction would have on the movement and range of the trebuchets is hard to determine. Not only would this need to be implemented in the mathematical model but it would also require experimental testing to find the magnitude of the friction forces involved. Clearly, this

is an extension that could be made to this paper which would make the models more realistic but also more complex.

Lastly, we also assumed the rope of the mangonel and trebuchet to be massless and rigid in order to reduce the number of coordinates. To assume the rope to be massless is not a very improper assumption as compared to the counterweight it is very small. The rigidity of the rope, on the other hand, is not realistic. We see this when looking at slow-motion footage of a trebuchet firing [13]. In this video, we can see that during nearly the entire firing process the rope is not fully extended. This changes the coordinates of the projectile as well as the projectile's influence on the rest of the system. Again, the influence of this assumption is difficult to check as we were unable to find any studies which modelled a rope. Therefore, it would be interesting to model this and compare the subsequent results.

To conclude, albeit the models we proposed in this paper have several simplifications that ought to be addressed to make them more realistic we can think of these models as proper and insightful tools. These tools can be used to look at the influence of the differences between the different types of catapults we have taken a look at.

9

Conclusion

In this report, we have taken a look at three different types of trebuchets: the seesaw, the traction trebuchet or mangonel, and the counterweight trebuchet. We have discussed the theory needed to develop the models that were presented in chapters 3, 4, and 5. Moreover, we have also calculated a lower bound for the dimensions of the main beam needed to prevent it from breaking based on a static state.

We have seen that the mangonel and trebuchet improved on the seesaw by increasing the range roughly sixfold. The maximum range of the seesaw was 28.3m with a release angle of 2.675 rad while the mangonel had a maximum range of 196.1m with a release angle of 2.196 rad. This increase can be accredited to the sling that was added compared to the seesaw. We, however, modelled the rope as a beam which we saw was not very realistic when comparing it to video footage.

When also adding the hinged counterweight, leading to the trebuchet, we found that the range had not increased but rather decreased. The trebuchet, namely, had a maximum range of 193.0m with a release angle of 2.396 rad. This is surprising as, according to historical accounts, the trebuchet is supposed to shoot further than the mangonel. We believe this discrepancy can be explained by the fact that we have not looked at the optimal lengths for the different catapults. Perhaps, when comparing the optimal mangonel with the optimal trebuchet we would find that the trebuchet does indeed fire farther than the mangonel.

If we look more closely at how the angles of the systems evolve over time we see that the seesaw and mangonel look very similar while the trebuchet differs significantly. We believe this is due to the mass of the counterweight being large compared to the projectile. Therefore a change in the coordinates of the counterweight has more effect on how the angles evolve than a change in the coordinates of the projectile.

Lastly, we also considered the thickness of the main beam needed to prevent it from breaking in a static case. We found that the beam needed to be at least 18.7 cm to prevent it from breaking. However, for the dynamic case, the beam would most likely need to be thicker to prevent it from breaking.

Bibliography

[1] C. Carrillo, *The trebuchet*, Sep. 2005. [Online]. Available: https://illumin.usc.edu/the-trebuchet/.

[2] J. Liang, *Chinese siege warfare: Mechanical Artillery & Siege Weapons of Antiquity, an illustrated history*. Leong Kit Meng, 2006.

[3] M. Denny, "Siege engine dynamics," *European Journal of Physics*, vol. 26, no. 4, pp. 561–577, Apr. 2005. DOI: 10.1088/0143-0807/26/4/002. [Online]. Available: https://doi.org/10.1088/0143-0807/26/4/002.

[4] P. E. Chevedden, L. Eigenbrod, V. Foley, and W. Soedel, "The trebuchet," *Scientific American*, vol. 273, no. 1, pp. 66–71, Jul. 1995. [Online]. Available: https://www.scientificamerican.com/article/the-trebuchet/.

[5] *Trebuchet drawing catapult - trebuchet dog*. [Online]. Available: https://www.seekpng.com/ipng/u2w7e6e6i1e6i1r5_trebuchet-drawing-catapult-trebuchet-dog/.

[6] Sep. 2006. [Online]. Available: https://commons.wikimedia.org/wiki/File:Mangonneau4.png.

[7] J. R. Taylor, *Classical mechanics*. University Science Books, 2005.

[8] T. D. OpenCourseWare. [Online]. Available: https://ocw.tudelft.nl/course-exercises/exercise-shear-force-bending-moment-diagrams-solution/.

[9] *Houteigenschappen sterktegegevens van gezaagd hout en ... - houtinfo.nl*. [Online]. Available: https://houtinfo.nl/sites/default/files/Infoblad_Houteigenschappen_Sterktegegevens_mrt2014_0.pdf.

[10] A. Huisman, "Het rendement van verschillende ontwerpen van de trebuchet bij het afschieten van een voorwerp," 2020.

[11] R. de Jong, "Modelling the movements of a counterweight trebuchet while firing," 2020.

[12] D. B. Siano, *Trebuchet mechanics*, 2001.

[13] *Launching my 1,000-lb Medieval Trebuchet by Myself*. Dawesome21, Sep. 2019. [Online]. Available: https://www.youtube.com/watch?v=PzQCcWVsiNw.

A

Appendix

In this section we will show the calculations which have not been presented in chapters 3, 4, 5, and 7. The calculations for the motion of the seesaw have been presented fully in chapter 3 and thus we will only show the calculations of the internal stresses for the seesaw. For the mangonel and the trebuchet, we will show the calculations in full, albeit with less commentary. For the definitions of the coordinates for the different catapults, we refer back to the corresponding chapters. The code used for this paper can be requested.

Seesaw

Internal stresses

For how the forces are defined we refer to figure 7.1. Note that we define forces in the $-\hat{y}, \hat{\theta}$ directions as positive and forces in the $\hat{y}, -\hat{\theta}$ directions as negative. We have that

$$F_{g,m} = mg \tag{A.1}$$
$$F_{g,m_b} = m_b g \tag{A.2}$$
$$F_{g,M} = Mg \tag{A.3}$$
$$F_r = -F_{g,m} - F_{g,m_b} - F_{g,M} \tag{A.4}$$

The components perpendicular to the main beam are given by

$$F_{g,m\perp} = \sin(\theta) mg \tag{A.5}$$
$$F_{g,m_b\perp} = \sin(\theta) m_b g \tag{A.6}$$
$$F_{g,M\perp} = \sin(\theta) Mg \tag{A.7}$$
$$F_{r\perp} = -\sin(\theta)(F_{g,m} + F_{g,m_b} + F_{g,M}) \tag{A.8}$$

However, as we assume the beam to be horizontal $\theta = \frac{1}{2}\pi$ and therefore $F_{i_\perp} = F_i$. Looking at figure 7.2 we see that

$$M_1 = -F_{g,m\perp} L_2 - \frac{1}{2} L_2^2 \frac{F_{g,m_b\perp}}{L_1 + L_2} \tag{A.9}$$
$$M_2 = -F_{g,m\perp} L_2 + F_{g,M\perp}(L_1 + L_M) + \frac{1}{2}(L_1^2 + L_2^2)\frac{F_{g,m_b\perp}}{L_1 + L_2} \tag{A.10}$$

Substituting this in eventually results in

$$M_1 = g\left(mL_2 + \frac{1}{2}\frac{m_b}{L_1 + L_2} L_2^2\right) \tag{A.11}$$
$$M_2 = g\left(M(L_1 + L_M) - mL_2 + \frac{1}{2} m_b (L_1 - L_2)\right) \tag{A.12}$$

Therefore, the maximum bending moment is given by the maximum absolute value of both bending moments.

Mangonel

Phase I

During this phase we assume the projectile is moving through a trough on the ground. Therefore, $y_m = -H$ which can be rewritten as a holonomic constraint.

$$f(\theta,\alpha) = H - \cos(\theta)L_2 + \cos(\alpha+\theta)L_3 = 0 \tag{A.13}$$

By using the method of the Lagrange multiplier we get for all coordinates q_i

$$\frac{d}{dt}\frac{\delta\mathscr{L}}{\delta\dot{q}_i} - \frac{\delta\mathscr{L}}{\delta q_i} - \lambda(t)\frac{\delta f}{\delta q_i} = 0 \tag{A.14}$$

The kinetic and potential energies are given by

$$T = \frac{1}{2}\dot{\theta}^2\left(M(L_1+L_M)^2 + I_b + m(L_2^2+L_3^2) - 2m\cos(\alpha)L_2L_3\right) + \frac{1}{2}m\dot{\alpha}^2L_3^2 + \dot{\alpha}\dot{\theta}m(L_3^2 - \cos(\alpha)L_2L_3)$$

$$U = g\cos(\theta)\left(M(L_1+L_M) - m_bL_b - mL_2\right) + \cos(\alpha+\theta)mgL_3$$

which is simply obtained by substituting the coordinates into the standard definitions of the kinetic and potential energy. This gives us our Lagrangian

$$\begin{aligned}\mathscr{L} = T - U = \frac{1}{2}\dot{\theta}^2\left(M(L_1+L_M)^2 + I_b + m(L_2^2+L_3^2) - 2m\cos(\alpha)L_2L_3\right) + \frac{1}{2}m\dot{\alpha}^2L_3^2 \\ +\dot{\alpha}\dot{\theta}m(L_3^2 - \cos(\alpha)L_2L_3) - g\cos(\theta)\left(M(L_1+L_M) - m_bL_b - mL_2\right) - \cos(\alpha+\theta)mgL_3\end{aligned} \tag{A.15}$$

Now by substituting equation A.15 into equation A.14 and using f as described earlier we get the following two equations.

$$\begin{aligned}\ddot{\theta}\left(M(L_1+L_M)^2 + I_b + m(L_2^2+L_3^2) - 2m\cos(\alpha)L_2L_3\right) + \ddot{\alpha}(mL_3^2 - \cos(\alpha)mL_2L_3) + \dot{\alpha}^2\sin(\alpha)mL_2L_3 \\ +2m\dot{\alpha}\dot{\theta}\sin(\alpha)L_2L_3 = \sin(\theta)\left(gM(L_1+L_M) - gm_bL_b - gmL_2 + \lambda L_2\right) + \sin(\alpha+\theta)(mgL_3 - \lambda L_3)\end{aligned} \tag{A.16}$$

$$\ddot{\alpha}mL_3^2 + \ddot{\theta}m(L_3^2 - cos(\alpha)L_2L_3) = \dot{\theta}^2m\sin(\alpha)L_2L_3 + \sin(\alpha+\theta)(mgL_3 - \lambda L_3) \tag{A.17}$$

We can write these equations as follows

$$\ddot{\theta}a_{11}(\alpha) + \ddot{\alpha}a_{12}(\alpha) + \lambda a_{13}(\theta,\alpha) = b_1(\alpha,\theta,\dot{\alpha},\dot{\theta}) \tag{A.18}$$

$$\ddot{\theta}a_{21}(\alpha) + \ddot{\alpha}a_{22} + \lambda a_{23}(\alpha,\theta) = b_2(\alpha,\theta,\dot{\theta}) \tag{A.19}$$

with

$$\begin{gathered}a_{11}(\alpha) = M(L_1+L_M)^2 + I_b + m(L_2^2+L_3^2) - 2m\cos(\alpha)L_2L_3 \\ a_{12}(\alpha) = -mL_3(\cos(\alpha)L_2 - L_3) \\ a_{13}(\theta,\alpha) = \sin(\alpha+\theta)L_3 - \sin(\theta)L_2 \\ b_1(\alpha,\theta,\dot{\alpha},\dot{\theta}) = \sin(\alpha+\theta)gmL_3 - \dot{\alpha}^2\sin(\alpha)mL_3L_2 - 2\dot{\alpha}\dot{\theta}\sin(\alpha)mL_2L_3 + g\sin(\theta)\left(M(L_1+L_M) - mL_2 - m_bL_b\right) \\ a_{21}(\alpha) = -mL_3(\cos(\alpha)L_2 - L_3) \\ a_{22} = mL_3^2 \\ a_{23}(\alpha,\theta) = \sin(\alpha+\theta)L_3 \\ b_2(\alpha,\theta,\dot{\theta}) = mL_3^2\left(\dot{\theta}^2\sin(\alpha)L_2 + g\sin(\alpha+\theta)\right)\end{gathered}$$

These are the coefficients as used in section 4.1. If we also take the second time derivative of equation A.13 we get

$$\ddot{f} = \ddot{\theta}\sin(\theta)L_2 + \dot{\theta}^2\cos(\theta)L_2 - \left(\ddot{\alpha}+\ddot{\theta}\right)\sin(\alpha+\theta)L_3 - \left(\dot{\alpha}+\dot{\theta}\right)^2\cos(\alpha+\theta)L_3 = 0 \tag{A.20}$$

Where we know this equals zero since f itself is equal to zero for all times. If we also write this equation like we did the others we get

$$\ddot{\theta} a_{31}(\alpha) + \ddot{\alpha} a_{32}(\alpha) + \lambda a_{33} = b_3(\alpha, \theta, \dot{\alpha}, \dot{\theta}) \tag{A.21}$$

with

$$\begin{aligned} a_{31}(\alpha) &= \sin(\theta) L_2 - \sin(\alpha + \theta) L_3 \\ a_{32}(\alpha) &= -\sin(\alpha + \theta) L_3 \\ a_{33} &= 0 \\ b_3(\alpha, \theta, \dot{\alpha}, \dot{\theta}) &= \left(\dot{\alpha} + \dot{\theta}\right)^2 \cos(\alpha + \theta) L_3 - \dot{\theta}^2 \cos(\theta) L_2 \end{aligned}$$

We can now write equations A.18, A.19, and 4.10 in a matrix representation.

$$\begin{pmatrix} a_{11} & a_{12} & a_{13} \\ a_{21} & a_{22} & a_{23} \\ a_{31} & a_{32} & a_{33} \end{pmatrix} \begin{pmatrix} \ddot{\theta} \\ \ddot{\alpha} \\ \lambda \end{pmatrix} = \begin{pmatrix} b_1 \\ b_2 \\ b_3 \end{pmatrix} \tag{A.22}$$

$$A \begin{pmatrix} \ddot{\theta} \\ \ddot{\alpha} \\ \lambda \end{pmatrix} = B$$

We can now get the formulas for $\ddot{\theta}$, $\ddot{\theta}$, and λ by multiplying the equation with the inverse of A if it exists. We know that the inverse of A exists if its determinant is different from zero.

$$\begin{aligned} \det(A) &= a_{11}(a_{22}a_{33} - a_{23}a_{32}) - a_{12}(a_{21}a_{33} - a_{23}a_{31}) + a_{13}(a_{21}a_{32} - a_{22}a_{31}) \\ &= -a_{11}a_{23}a_{32} + a_{12}a_{23}a_{31} + a_{13}(a_{21}a_{32} - a_{22}a_{31}) \\ &= a_{11}a_{23}^2 + a_{12}a_{23}a_{31} + a_{13}a_{21}a_{32} - a_{13}a_{22}a_{31}) \\ &= a_{11}a_{23}^2 + a_{12}a_{23}a_{31} + a_{12}a_{23}a_{31} + a_{22}a_{13}^2 \\ &= a_{11}a_{23}^2 + 2a_{12}a_{23}a_{31} + a_{22}a_{13}^2 \end{aligned} \tag{A.23}$$

The determinant is a function of θ and α. If we plot this function for $\theta, \alpha \in \{0, 2\pi\}$ we get figure A.1 when using the values as described in table 1.1.

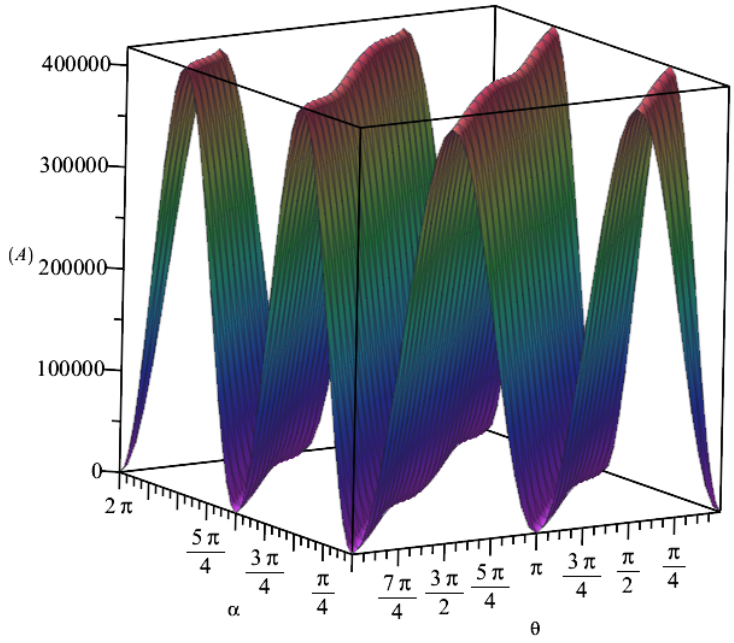

Figure A.1: The determinant of A for the given ranges of θ and α.

Despite the fact that the graph changes when we change the given values we have found that the zero points do not change. As we can see from the graph the zero points are at $(\theta,\alpha) \in \Big\{(0,0),(0,\pi),(0,2\pi),(\pi,0),(\pi,\pi),(\pi,2\pi),(2\pi,0).(2\pi,\pi),(2\pi,2\pi)\Big\}$. This makes sense since for $\theta+\alpha = n\pi$ with n any integer we have that $\sin(\theta+\alpha) = 0$. This results in $a_{23} = a_{32} = 0$ which reduces the determinant to

$$\begin{aligned} \det(A) &= a_{22}a_{13}^2 \\ &= m\sin^2(\theta)L_2^2L_3^2 \end{aligned} \tag{A.24}$$

This in turn is only zero for $\theta = k\pi$ with k any integer. This results in the different combinations of θ and α as mentioned previously. In phase I we start with $\alpha_0 = \frac{\pi}{2} - \theta_0$ or equivalently $\alpha_0 + \theta_0 = \frac{\pi}{2}$. Moreover, we can assume we leave phase I before $\theta+\alpha = \pi$. This is true because we leave this phase at the latest when the rope is hanging straight down since this would imply the projectile is hanging freely without dragging over the ground. If the rope hangs straight down we get $\alpha = \pi - \theta$ or equivalently $\theta+\alpha = \pi$. Therefore, during phase I we have found that A is indeed invertible.

Phase II

We transition to phase II when the magnitude of the gravitational force on the projectile is equal to the magnitude of the tension in the rope perpendicular to the y-axis. We can calculate the tension in the rope parallel to the q_i-axis as follows

$$F_{q_i} = -\lambda\frac{\delta f}{\delta q_i}$$

So we get

$$F_\theta = -\lambda\frac{\delta f}{\delta\theta} = -\lambda(\sin(\theta)L_2 - \sin(\alpha+\theta)L_3)$$

$$F_\alpha = -\lambda\frac{\delta f}{\delta\alpha} = \lambda\sin(\alpha+\theta)L_3$$

Therefore, the tension in the rope perpendicular to the y-axis is equal to

$$F_y = \sin(\theta)F_\theta - \sin(\alpha+\theta)F_\alpha = -\lambda(\sin(\theta)^2 L_2 - \sin(\alpha+\theta)\sin(\theta)L_3 + \sin(\alpha+\theta)^2 L_3) \tag{A.25}$$

which is obtained through some simple geometry. Therefore, as soon as $F_y \geq mg$ we can drop the constraint we introduced earlier. We drop the constraint by putting $\lambda = 0$ in equations A.17 and A.16. We can then write these two updated equations in matrix form.

$$\begin{pmatrix} a_{11} & a_{12} \\ a_{21} & a_{22} \end{pmatrix} \begin{pmatrix} \ddot{\theta} \\ \ddot{\alpha} \end{pmatrix} = \begin{pmatrix} b_1 \\ b_2 \end{pmatrix} \tag{A.26}$$

with the a_i and b_i the same as in phase I. We should again see if the inverse of A exists.

$$\begin{aligned} \det(A) &= a_{11}a_{22} - a_{12}a_{21} \\ &= a_{11}a_{22} - a_{12}^2 \end{aligned} \tag{A.27}$$

Putting this equal to zero we eventually obtain

$$\alpha = \cos^{-1}\left(\frac{\sqrt{m\left(ML_1^2 + 2ML_1L_M + ML_M^2 + mL_2^2 + \mathrm{I}_b\right)}}{mL_2}\right) \tag{A.28}$$

or

$$\alpha = \pi - \cos^{-1}\left(\frac{\sqrt{m\left(ML_1^2 + 2ML_1L_M + ML_M^2 + mL_2^2 + \mathrm{I}_b\right)}}{mL_2}\right) \tag{A.29}$$

We quickly see that the square root in equations A.28 and A.29 is larger than mL_2 and thus we get the inverse cosine of a number larger than 1 which is undefined. Therefore, we will never get that A has no inverse.

Phase III

Since for phase III the projectile is detached from the mangonel we are back at the simple seesaw. Therefore, the solutions for the mangonel of phase III are the same as the solutions for the seesaw. We discussed this in section 3.2. The motion of the projectile is different, however. At $\alpha = \alpha_r$ we have

$$\dot{x}_m = -\dot{\theta_r}\cos(\theta_r)L_2 + (\dot{\alpha_r} + \dot{\theta_r})\cos(\alpha_r + \theta_r)L_3$$

$$\dot{y}_m = \dot{\theta_r}\sin(\theta_r)L_2 - (\dot{\alpha_r} + \dot{\theta_r})\sin(\alpha_r + \theta_r)L_3$$

Since we assume there is no air resistance, $\ddot{x}_m = 0$ and $\ddot{y}_m = -g$. Therefore

$$x_m(t) = x_m(t_r) + t\dot{x}_m(t_r) = -\sin(\theta_r)L_2 + \sin(\alpha_r+\theta_r)L_3 - t\left(\dot{\theta}_r\cos(\theta_r)L_2 + (\dot{\alpha}_r+\dot{\theta}_r)\cos(\alpha_r+\theta_r)L_3\right)$$

$$y_m(t) = y_m(t_r) + t\dot{y}_m(t_r) = -\cos(\theta_r)L_2 + \cos(\alpha_r+\theta_r)L_3 + t\left(\dot{\theta}_r\sin(\theta_r)L_2 - (\dot{\alpha}_r+\dot{\theta}_r)\sin(\alpha_r+\theta_r)L_3\right)$$

where $\theta_r, \alpha_r, \dot{\theta}_r, \dot{\alpha}_r$ represent the values corresponding at the moment of release. Again solving for $y_m = -H$ gives us the time the object hits the ground, t_h. We can then find the range of the mangonel, namely $s = x_m(t = t_h)$

Trebuchet

Phase I

In phase I we can use the same constraint as we did for the mangonel, equation A.13. The kinetic energy is given by

$$\begin{aligned} T = &\frac{m\left(\left(-2L_2L_3\cos(\alpha) + L_2^2 + L_3^2\right)\dot{\theta}^2 - 2L_3\dot{\alpha}\left(\cos(\alpha)L_2 - L_3\right)\dot{\theta} + \dot{\alpha}^2L_3^2\right)}{2} + \\ &\frac{M\left(\left(\dot{\theta}\cos(\theta)L_1 + \left(\dot{\phi}-\dot{\theta}\right)\cos\left(\phi-\theta\right)L_M\right)^2 + \left(-\dot{\theta}\sin(\theta)L_1 + \left(\dot{\phi}-\dot{\theta}\right)\sin\left(\phi-\theta\right)L_M\right)^2\right)}{2} + \frac{\dot{\theta}^2\mathrm{I}_b}{2} \end{aligned} \tag{A.30}$$

And the potential energy is given by

$$U = g\left(M\left(\cos(\theta)L_1 - \cos\left(\phi-\theta\right)L_M\right) + m\left(-\cos(\theta)L_2 + \cos(\alpha+\theta)L_3\right) - m_b\cos(\theta)L_b\right) \tag{A.31}$$

This gives us our Lagrangian

$$\mathscr{L} = T - U \tag{A.32}$$

We can then use equation A.14 for the different coordinates giving us three equations, one for each coordinate. These equations can be calculated precisely which eventually gives them in the following forms.

$$\ddot{\theta}a_{11}(\alpha,\phi) + \ddot{\alpha}a_{12}(\alpha) + \ddot{\phi}a_{13}(\phi) + \lambda a_{14}(\theta,\alpha) = b_1(\theta,\alpha,\phi,\dot{\theta},\dot{\alpha},p\dot{h}i) \tag{A.33}$$

$$\ddot{\theta}a_{21}(\alpha) + \ddot{\alpha}a_{22} + \ddot{\phi}a_{23} + \lambda a_{24}(\theta,\alpha) = b_2(\theta,\alpha,\dot{\theta}) \tag{A.34}$$

$$\ddot{\theta}a_{31}(\phi) + \ddot{\alpha}a_{32} + \ddot{\phi}a_{33} + \lambda a_{34} = b_3(\theta,\phi,\dot{\theta}) \tag{A.35}$$

Lastly by differentiating equation A.13 twice we can write this too in the same form

$$\ddot{\theta}a_{41}(\theta,\alpha) + \ddot{\alpha}a_{42}(\theta,\alpha) + \ddot{\phi}a_{43} + \lambda a_{44} = b_4(\theta,\alpha,\dot{\theta},\dot{\alpha}) \tag{A.36}$$

with

$a_{11}(\alpha,\phi) = M\left(L_M^2 + L_1^2\right) + m\left(L_2^2 + L_3^2\right) + \mathrm{I}_b - 2\cos(\alpha)mL_2L_3 - 2\cos\left(\phi\right)ML_1L_M$
$a_{12}(\alpha) = -mL_3\left(\cos(\alpha)L_2 - L_3\right)$
$a_{13}(\phi) = -ML_M^2 + ML_1L_M\cos\left(\phi\right)$
$a_{14}(\theta,\alpha) = -\sin(\theta)L_2 + \sin(\alpha+\theta)L_3$
$b_1(\theta,\alpha,\phi,\dot{\theta},\dot{\alpha},\dot{\phi}) = \sin(\phi)\dot{\phi}ML_1L_M\left(\dot{\phi}-2\dot{\theta}\right) - \sin(\alpha)\dot{\alpha}mL_2L_3\left(\dot{\alpha}+2\dot{\theta}\right) + \sin(\theta)g\left(ML_1 - mL_2 - m_bL_b\right) + \sin(\phi-\theta)g\left(ML_M + mL_3\right)$
$a_{21}(\alpha) = -mL_3\left(\cos(\alpha)L_2 - L_3\right)$
$a_{22} = mL_3^2$
$a_{23} = 0$
$a_{24}(\theta,\alpha) = \sin(\alpha+\theta)L_3$
$b_2(\theta,\alpha,\dot{\theta}) = mL_3\left(\dot{\theta}^2\sin(\alpha)L_2 + \sin(\alpha+\theta)g\right)$
$a_{31}(\phi) = -ML_M^2 + ML_1L_M\cos\left(\phi\right)$
$a_{32} = 0$
$a_{33} = ML_M^2$
$a_{34} = 0$
$b_3(\theta,\phi,\dot{\theta}) = ML_M\left(\dot{\theta}^2\sin\left(\phi\right)L_1 - \sin\left(\phi-\theta\right)g\right)$
$a_{41}(\theta,\alpha) = \sin(\theta)L_2 - \sin(\alpha+\theta)L_3$
$a_{42}(\theta,\alpha) = -\sin(\alpha+\theta)L_3$
$a_{43} = 0$
$a_{44} = 0$
$b_4(\theta,\alpha,\dot{\theta},\dot{\alpha}) = -\dot{\theta}^2\cos(\theta)L_2 + \left(\dot{\alpha}+\dot{\theta}\right)^2\cos(\alpha+\theta)L_3$

We can then write this as a matrix equation.

$$\begin{pmatrix} a_{11} & a_{12} & a_{13} & a_{14} \\ a_{21} & a_{22} & a_{23} & a_{24} \\ a_{31} & a_{32} & a_{33} & a_{34} \\ a_{41} & a_{42} & a_{43} & a_{44} \end{pmatrix} \begin{pmatrix} \ddot{\theta} \\ \ddot{\alpha} \\ \ddot{\phi} \\ \lambda \end{pmatrix} = \begin{pmatrix} b_1 \\ b_2 \\ b_3 \\ b_4 \end{pmatrix} \tag{A.37}$$

$$A\begin{pmatrix}\ddot{\theta}\\ \ddot{\alpha}\\ \ddot{\phi}\\ \lambda\end{pmatrix} = B$$

We can again get the direct formulae for $\ddot{\theta}, \ddot{\alpha}, \ddot{\phi}$, and λ by multiplying equation 5.2 with the inverse of A if it exists. The inverse of A exists if the determinant is unequal to zero. After some tedious calculations we eventually get to

$$\det(A) = \sin(\alpha+\theta)\Big(-M^2\sin(\alpha+\theta)\cos\left(\phi\right)^2 L_1^2L_3^2L_M^2 - 2Mm\sin(\theta)\cos(\alpha)L_2^2L_3^2L_M^2 + M^2\sin(\alpha+\theta)L_1^2L_3^2L_M^2 + M\sin(\alpha+\theta)mL_2^2L_3^2L_M^2 + M\sin(\alpha+\theta)\mathrm{I}_bL_3^2L_M^2\Big) + M\sin(\theta)^2mL_2^2L_3^2L_M^2 \quad \text{(A.38)}$$

We then see the determinant will be equal to zero for $\alpha+\theta = n\pi$ with n any integer and $\theta = k\pi$ with k any integer. This gives us that both θ and α have to be either 0 or π. Note that the value of ϕ is free. We have checked this numerically which produced the isosurface where $\det(A) = 0$ shown in figure A.2. Note that although the values of $\det(A)$ will change with different parameters, the isosurface where $\det(A) = 0$ will be the same.

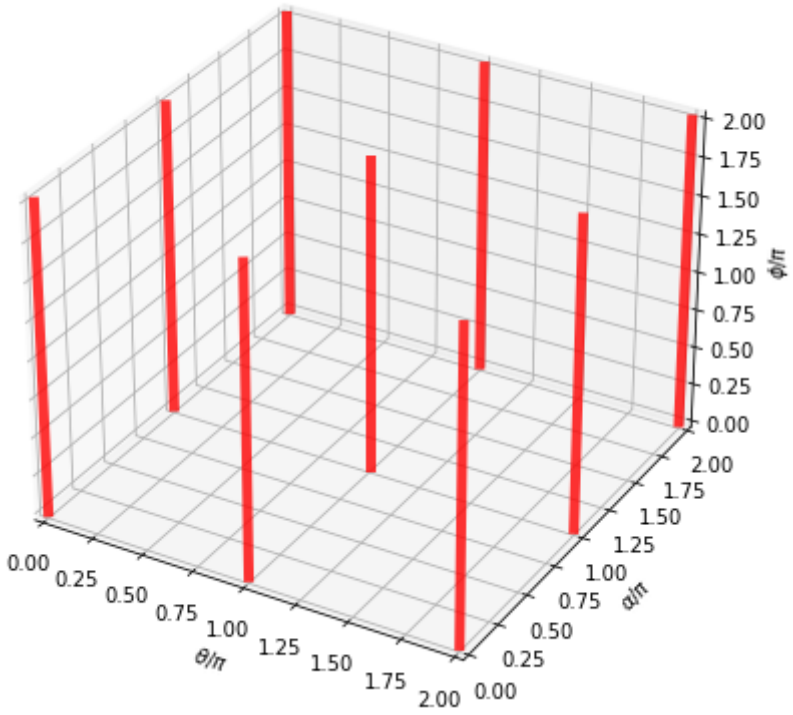

Figure A.2: The isosurface where the determinant of A as defined in equation A.38 is equal to zero.

Similar to as we discussed for phase I of the mangonel we leave this phase at the latest when $\theta+\alpha = \pi$ and start with $\theta, \alpha > 0$ and $\dot{\theta}, \dot{\alpha} \geq 0$. Therefore, we have during this phase that θ and α will never both be 0 or π and thus that the inverse of this matrix exists during this phase.

Phase II

Since the constraint force is the same as for the mangonel we still get that when equation A.25 is equal and opposite to the gravitational force mg we drop the constraint. We do this by putting $\lambda = 0$ in equations A.33, A.34, and A.35. We can write these updated equations again in a matrix representation.

$$\begin{pmatrix}a_{11} & a_{12} & a_{13}\\ a_{21} & a_{22} & a_{23}\\ a_{31} & a_{32} & a_{33}\end{pmatrix}\begin{pmatrix}\ddot{\theta}\\ \ddot{\alpha}\\ \ddot{\phi}\end{pmatrix} = \begin{pmatrix}b_1\\ b_2\\ b_3\end{pmatrix} \quad \text{(A.39)}$$

$$A\begin{pmatrix}\ddot{\theta}\\ \ddot{\alpha}\\ \ddot{\phi}\end{pmatrix} = B$$

with a_i and b_i the same as in phase I. If the determinant of A is unequal to zero its inverse exists and we can thus find the direct formulae for $\ddot{\theta}, \ddot{\alpha}$, and $\ddot{\phi}$.

$$\begin{aligned}\det(A) &= a_{11}(a_{22}a_{33} - a_{23}a_{32}) - a_{12}(a_{21}a_{33} - a_{23}a_{31}) + a_{13}(a_{21}a_{32} - a_{22}a_{31}) \\ &= a_{11}a_{22}a_{33} - a_{12}^2 a_{33} - a_{22}a_{13}^2\end{aligned} \tag{A.40}$$

This eventually, after some tedious calculations, simplifies to

$$\det(A) = -MmL_3^2L_M^2\left(M\cos\left(\phi\right)^2 L_1^2 + \cos\left(\alpha\right)^2 mL_2^2 - ML_1^2 - mL_2^2 - \mathrm{I}_b\right) \tag{A.41}$$

We see the determinant can never become zero since is it bounded above by $MmL_3^2L_M^2\left(ML_1^2 + mL_2^2 + \mathrm{I}_b\right)$ for $\alpha, \phi = n\pi + \frac{1}{2}\pi$ and below by $MmL_3^2L_M^2\mathrm{I}_b$ for $\alpha, \phi = n\pi$ with n any integer. Therefore, the determinant can never become zero and thus the inverse of A always exists.

Phase III

For phase III we, just like with the mangonel, can ignore the rope since the projectile is detached from the trebuchet. This changes both the kinetic and potential energy and with it the Lagrangian.

$$T = \frac{M\theta^2L_1^2}{2} - M\theta\phi L_M^2 + \frac{\theta^2\mathrm{I}_b}{2} - M\theta^2L_1L_M\cos\left(\phi\right) + M\theta\phi L_1L_M\cos\left(\phi\right) + \frac{M\theta^2L_M^2}{2} + \frac{M\phi^2L_M^2}{2} \tag{A.42}$$

$$U = g\left(M\left(\cos\left(\theta\right)L_1 - \cos\left(\phi - \theta\right)L_M\right) - m_b\cos\left(\theta\right)L_b\right) \tag{A.43}$$

Substracting equation A.43 from A.42 gives us our Lagrangian. By applying the Euler-Lagrange equation (2.8) for the different coordinates we get the following two equations.

$$\ddot{\theta}a_{11}(\alpha,\phi) + \ddot{\phi}a_{13}(\phi) = b_1(\theta,\alpha,\phi,\dot{\theta},\dot{\alpha},p\dot{h}i) \tag{A.44}$$

$$\ddot{\theta}a_{31}(\alpha,\phi) + \ddot{\phi}a_{33}(\phi) = b_3(\theta,\alpha,\phi,\dot{\theta},\dot{\alpha},p\dot{h}i) \tag{A.45}$$

with

$$\begin{aligned}a_{11}(\phi) &= \mathrm{I}_b + ML_M^2 + ML_1^2 - 2ML_1L_M\cos\left(\phi\right) \\ a_{13}(\phi) &= -ML_M^2 + ML_1L_M\cos\left(\phi\right) \\ b_1(\theta,\phi,\dot{\theta},\dot{\phi}) &= \sin(\phi)\dot{\phi}ML_1L_M\left(\dot{\phi} - 2\dot{\theta}\right) + \sin(\theta)g\left(ML_1 - m_bL_b\right) + \sin(\phi-\theta)gML_M \\ a_{31}(\phi) &= -ML_M^2 + ML_1L_M\cos\left(\phi\right) \\ a_{33} &= ML_M^2 \\ b_3(\theta,\phi,\dot{\theta}) &= ML_M\left(\dot{\theta}^2\sin\left(\phi\right)L_1 - \sin\left(\phi-\theta\right)g\right)\end{aligned}$$

Notice that a_{ij} and b_i are the same as for phase II but with $m = 0$. We can now write the equations in matrix form.

$$\begin{pmatrix}a_{11} & a_{13}\\ a_{31} & a_{33}\end{pmatrix}\begin{pmatrix}\ddot{\theta}\\ \ddot{\phi}\end{pmatrix} = \begin{pmatrix}b_1\\ b_3\end{pmatrix} \tag{A.46}$$

$$A\begin{pmatrix}\ddot{\theta}\\ \ddot{\alpha}\\ \ddot{\phi}\end{pmatrix} = B$$

We again have to check if the determinant of A is unequal to zero.

$$\begin{aligned}\det(A) &= a_{11}a_{33} - a_{13}a_{31} \\ &= a_{11}a_{33} - a_{13}^2 \\ &= -M^2\cos\left(\phi\right)^2L_1^2L_M^2 + M^2L_1^2L_M^2 + M\mathrm{I}_bL_M^2\end{aligned} \tag{A.47}$$

We quickly see that the determinant is bounded above by $M^2L_1^2L_M^2 + M\mathrm{I}_bL_M^2$ for $\phi = n\pi + \frac{1}{2}\pi$ and below by $M\mathrm{I}_bL_M^2$ for $\phi = n\pi$ with n any integer. Therefore, the determinant will never become equal to zero and thus the inverse of A will always exist. Since the coordinates of the projectile are the same as for the mangonel so is the trajectory of the projectile in phase III.